

Review

Titanium Dioxide/Graphene and Titanium Dioxide/Graphene Oxide Nanocomposites: Synthesis, Characterization and Photocatalytic Applications for Water Decontamination

Amr Tayel ^{1,*}, Adham R. Ramadan ¹ and Omar A. El Seoud ² 

¹ Department of Chemistry, The American University in Cairo, P.O. Box 74, New Cairo 11835, Egypt; aramadan@aucegypt.edu

² Institute of Chemistry, The University of São Paulo, P.O. Box 26077, São Paulo 05513-970, Brazil; elseoud.usp@gmail.com

* Correspondence: amr2tayel@aucegypt.edu; Tel.: +20-1-000-288-385

Received: 25 September 2018; Accepted: 18 October 2018; Published: 24 October 2018



Abstract: The use of titanium dioxide, TiO₂ as a photocatalyst in water decontamination has witnessed continuous interest due to its efficiency, stability, low toxicity and cost-effectiveness. TiO₂ use is limited by its large band gap energy leading to light absorbance in the UV region of the spectrum, and by the relatively fast rate of recombination of photogenerated electrons and positive holes. Both limitations can be mitigated by using carbon-TiO₂ nanocomposites, such as those based on graphene (G) and graphene oxide (GO). Relative to bare TiO₂, these nanocomposites have improved photocatalytic activity and stability under the UV–visible light, constituting a promising way forward for improved TiO₂ photocatalytic performance. This review focuses on the recent developments in the chemistry of TiO₂/G and TiO₂/GO nanocomposites. It addresses the mechanistic fundamentals, briefly, of TiO₂ and TiO₂/G and TiO₂/GO photocatalysts, the various synthesis strategies for preparing TiO₂/G and TiO₂/GO nanocomposites, and the different characterization techniques used to study TiO₂/G and TiO₂/GO nanocomposites. Some applications of the use of TiO₂/G and TiO₂/GO nanocomposites in water decontamination are included.

Keywords: TiO₂; graphene; graphene oxide; surface properties; photocatalytic applications; water decontamination

1. Introduction

Addressing environmental pollution is a top priority worldwide [1,2]. In this respect, the remediation of wastewater from organic contaminants presents an increasingly urgent need in order to address the associated environmental and public health negative impacts, and the surge in water reuse needs due to global water shortages. The textile dyeing and finishing industry is one of the most chemically intensive sectors and is ranked as number two polluter of clean water, after agriculture [3]. The potential magnitude of the environmental problems associated with wastewater from this industrial sector can be appreciated by considering the large number, 100,000, of commercially available dyes, with over 7×10^5 tons of dye-stuff produced annually [4]. This, coupled with the incomplete degradation of these dyes due to their chemical stability, contribute to the significance of this type of pollution. Thus, reactive azo dyes that constitute 65–70% of all dyes produced [5], are not totally degraded by conventional wastewater treatment processes that involve light, chemicals or activated sludge [6–8]. Additionally, a fraction of these dyes (estimated between 2% and 10%) is discharged directly into aqueous effluents or lost during the textile dyeing process [9].

Removal of these contaminants using efficient and environmentally-friendly methods is crucial [10,11]. Various strategies are utilized for wastewater treatment such as reverse osmosis, ultrafiltration, evaporation and solvent extraction. However, these techniques remove contaminants from water without converting them into harmless end-products [12]. Complete degradation can be readily achieved by oxidation, either chemically or photochemically [13]. The aim of any oxidative process is to produce and use hydroxyl free radical (HO^\bullet) as a strong oxidant to degrade pollutants. Hydrogen peroxide is used as an oxidant after activation, by metal ions for example as in Fenton reagent [6], or by UV radiation [14].

Photocatalytic processes, including oxidation, provide an attractive alternative because they rely on using the radiation energy to promote the required degradation. Examples of photocatalytic processes are dye decomposition [15], water/air purification [16,17], filtration [18] and self-cleaning applications [19]. Specifically, TiO_2 has been used as a photocatalyst in wastewater treatment of dyes [12,20–22], hormones [23], pharmaceuticals [24,25], industrial wastewater [26], and microbial disinfection [27–29].

Though anatase and rutile are the commonly used crystal phases of TiO_2 in photocatalytic reactions, amorphous TiO_2 has also been reported for enhanced photocatalytic activity as a result of surface defects leading to higher electron transfer [30–32]. This has also been reported for anatase [33–37]. The measured photocatalytic activity is found to depend not only on the crystal phases used, and the modifications carried out on the photocatalyst, but also the contaminant undergoing photocatalysis [38–40].

Rutile, the more thermodynamically stable polymorph, has a band gap value of ca. 3.0 eV. On the other hand, anatase has higher charge-carrier mobility and greater photocatalytic activity [41]. Its use is associated, however, with the rapid re-combination between the positive holes on the TiO_2 surface and the photoinduced electrons, which reduces the overall photocatalytic efficiency. Moreover, its band gap is ca. 3.2 eV, meaning that it absorbs light radiation in the UV region of the solar spectrum, that represents 4% of the solar radiation [42–44]. Therefore, it is essential to decrease the energy of this band gap, leading to light absorption by TiO_2 in the visible region that represents 42% of solar radiation. This means a large enhancement in the light harvesting power of TiO_2 -based material [45,46].

The photocatalytic activity of TiO_2 can be improved by doping with transition metals such as V, Ni and Cr, or with nonmetals such as N and S. Carbon- TiO_2 composites, including graphene (G) and graphene oxide (GO), provide enhanced photocatalytic activity and stability under UV light irradiation, relative to TiO_2 [47–49]. Although TiO_2 doping might lead to higher photocatalytic activity [50–55], increased surface area with improved contaminant adsorption are advantages of TiO_2/G and TiO_2/GO composites [56–59]. Furthermore, TiO_2/G and TiO_2/GO exhibit comparable photostability to doped TiO_2 [55,60–62].

Graphene is a carbon allotrope that exists of one atom thick layers arranged in a honeycomb two-dimensional (2D) crystal structure. It has shown remarkable optical, electrical, catalytic, thermal, and mechanical properties leading to numerous applications [63]. Graphene has very high electron mobility and a high surface area making it an attractive material for photocatalysis applications [64,65].

Graphene oxide is produced by oxidation of high purity graphite. It possesses unique properties that are different from those of G due to the existence of various oxygenated functional groups on the surface of GO sheets. These properties include attractive optical properties (GO is used as fluorescence labels [66]), high dispersibility in various polar solvents and the ability to attach diverse molecular structures on its surface, e.g., by hydrogen bonding. These properties facilitate the adsorption of various molecular structures on its surface, leading to a better control of the size, and the shape of the formed structures. In addition, the average cost of producing GO is smaller compared with those of G and several other nanomaterials. These remarkable properties are extremely beneficial in making TiO_2/GO nanocomposites. The relative hydrophilicity of GO, due to the highly oxygenated surface facilitates its interaction with aqueous dispersions of TiO_2 , leading to the formation of strong,

chemically-bonded TiO₂/GO nanocomposites. This good dispersibility in aqueous solutions is not easily achievable with G without adding a dispersant [67,68].

Figure 1 shows the increase in the number of scientific publications and citations regarding TiO₂/G and TiO₂/GO nanocomposites during the past decade. The significant increase for the last five years is a clear evidence of the significance of the subject.

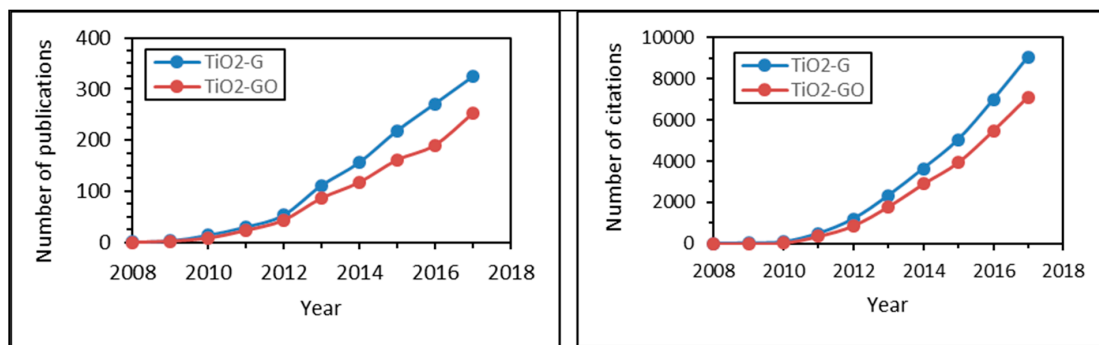


Figure 1. Total number of publications with the keywords “Titanium dioxide and graphene” and “Titanium dioxide and graphene oxide”, based on data from Web of Science database.

Figure 2 illustrates the main mechanistic steps for TiO₂ photocatalytic activity. The photo-reduction phase involves the excitation of electrons from the valence band (VB) to the conduction band (CB) with the formation of positive holes (h⁺) after the absorption of light photons of proper energy. These photo-generated electrons and positive holes emerge to the TiO₂ surface and react with the adsorbed species. The photo-generated electrons react with the adsorbed oxygen to form hydroxyl radicals (OH•) and super-oxide radicals (O₂^{•-}). The formed radicals are highly reactive and represent the main intermediates in the oxidation of organic pollutants. Moreover, adsorbed hydroxyl ions and water molecules are oxidized by the positive holes formed in the CB to give hydroxyl radicals (OH•) which, in turn, degrade the organic pollutants to harmless end-products. This is known as the photo-oxidation phase [69,70].

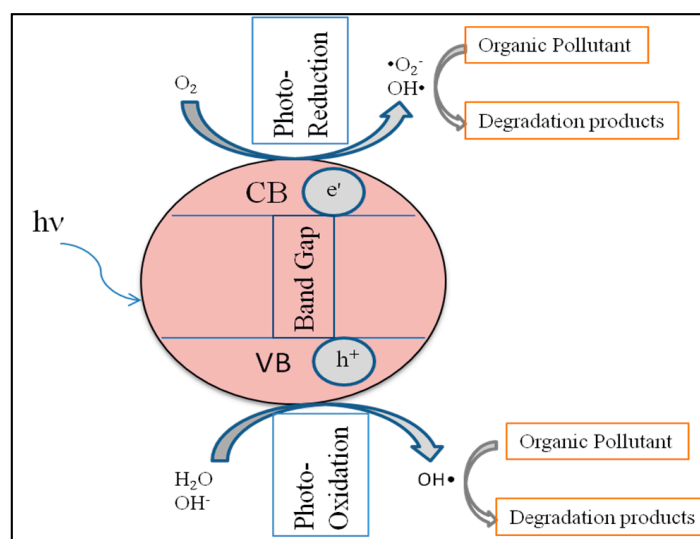


Figure 2. Principles of TiO₂ photocatalysis.

The main steps involved in TiO₂ photocatalysis are summarized in Equations (1)–(6).





Recently, G and GO have been the subject of various studies where they were used to form composite materials with TiO₂ with improved photocatalytic performance. This improvement is achieved by one or more of the following schemes: (1) Enhancement of the surface area of TiO₂ due to its interaction with the two-dimensional matt structure of G and GO; (2) Enhancement of the adsorption of aromatic contaminants due to their strong π - π interactions with the aromatic network of G and GO; and (3) Decrease of the rate of re-combination between the positive holes and the photogenerated electrons due to the substantial electronic conductivity of G and GO that act as an electron sink for the photo-generated electrons on the surface of TiO₂ [71–74].

The enhancement of the photocatalytic activity of TiO₂ using G and GO is illustrated in Figures 3 and 4. In addition, some reports explained the role of G itself in the photodegradation of methylene blue (MB) using TiO₂/G nanocomposites through the formation of OH[•] using the photogenerated electrons on its surface [75,76].

Reviews on TiO₂ photocatalysis have recently been published by Schneider [1], Xu [77], Dahl [78], and Fang [79] and on G-based photocatalysts by Chowdhury [70], Upadhyay [80], and Cao [81]. Comprehensive reviews on TiO₂/G and TiO₂/GO composites were presented by Tan [75], Torres [82], energy applications [83], and environmental applications [84]. Considering the significant increase in the number of publications on this topic, shown in Figure 1, together with the number of citations of these publications, we consider this updated review as timely and of wide interest.

In this respect, this review aims to update researchers in the field of TiO₂/G and TiO₂/GO nanocomposites with the most recent developments, as well as providing newcomers to this rapidly growing field with an up to date summary on TiO₂/G and TiO₂/GO nanocomposites synthesis, characterization, and applications. The detailed characterization section, which is unique to this review, aims at providing a guide to the different commonly used techniques for the elucidation of macroscopic and microscopic properties of TiO₂/G and TiO₂/GO nanocomposites. Additionally, some photocatalytic applications of TiO₂/G and TiO₂/GO nanocomposites in wastewater treatment are summarized, focusing on recent applications. A summary of the TiO₂/G and TiO₂/GO synthesis, characterization, and photocatalytic applications for the decomposition of water contaminants is given in Table S1 of supporting information.

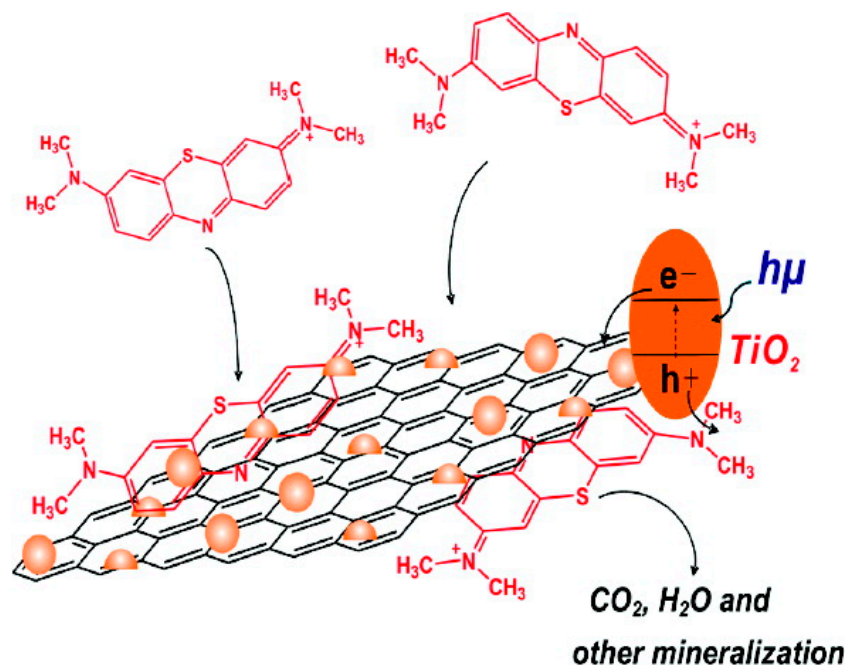


Figure 3. Improved photodegradation of methylene blue at the surface of TiO_2/G nanocomposites. The improvement is due to a combination of enhanced MB adsorption due to dye- TiO_2/G hydrophobic interactions and increased photogenerated electrons-positive holes lifetime. Reprinted with permission from reference [71]. Copyright 2010 American Chemical Society.

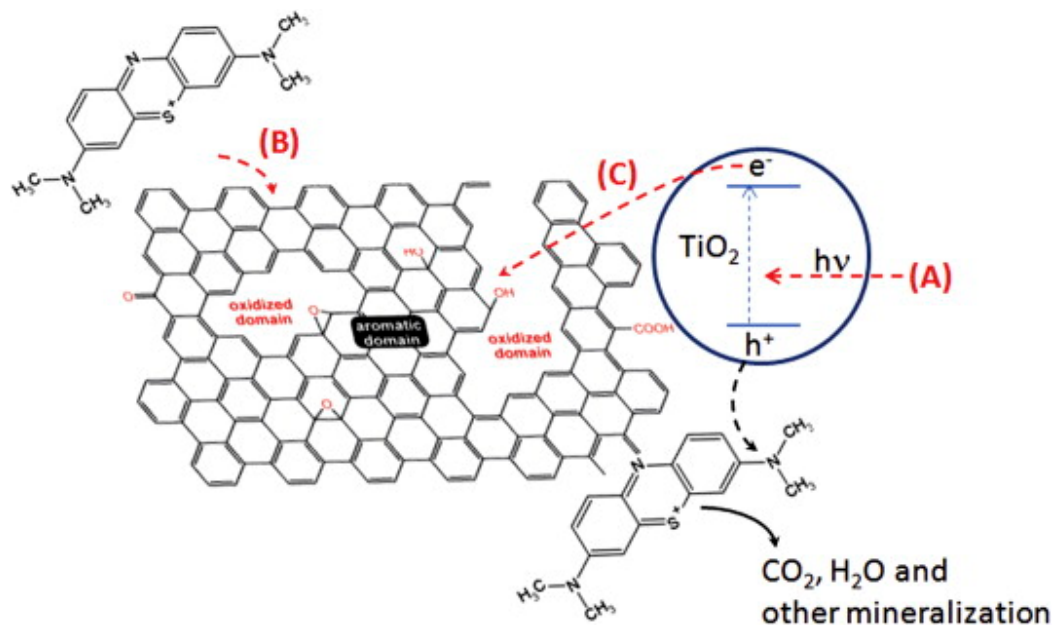


Figure 4. TiO_2/GO nanocomposites and mechanisms of MB photo-decomposition (A) light absorption (B) dye adsorption (C) electron transfer and charge separation. The improvement in degradation is due to dye- TiO_2/GO hydrophobic and dipolar interactions and increased photogenerated electrons-positive holes lifetime. Reprinted with permission from reference [72]. Copyright 2011 Elsevier.

2. Synthesis of TiO_2/G and TiO_2/GO Nanocomposites

The synthesis techniques used for the preparation of TiO_2/G and TiO_2/GO nanocomposites include hydrothermal (HT), solvothermal (ST), mechanical mixing with or without sonication, sol-gel techniques, deposition techniques of liquids (LPD), aerosol (AD), chemical vapor (CVD), spin coating

and electrospinning. Unless otherwise specified, PTFE-lined autoclaves are employed for heating reaction mixtures above the boiling point of the solvent employed.

2.1. The Hydrothermal (HT) Method

The term hydrothermal synthesis refers to a technique for growing crystals from an aqueous solution in an autoclave at high temperature and pressure. The key steps in the HT preparation of TiO_2/G and TiO_2/GO nanocomposites are illustrated in Figure 5. Elevated pressures allow the use of low boiling point solvents, in particular, water. This use is beneficial as the majority of high boiling point solvents, such as dimethyl sulfoxide (DMSO), are either expensive or have some toxicity. The use of elevated temperatures produces high-quality crystals of the desired nanomaterial. HT synthesis allows the control of the composition and quality of the formed nanocrystals. However, the inability to monitor material crystal growth (in the autoclave) and the equipment cost are the main limitations associated with this method [85–88]. The HT reaction is used for the formation of the TiO_2/G nanocomposites and in the partial reduction of the GO into G [89].

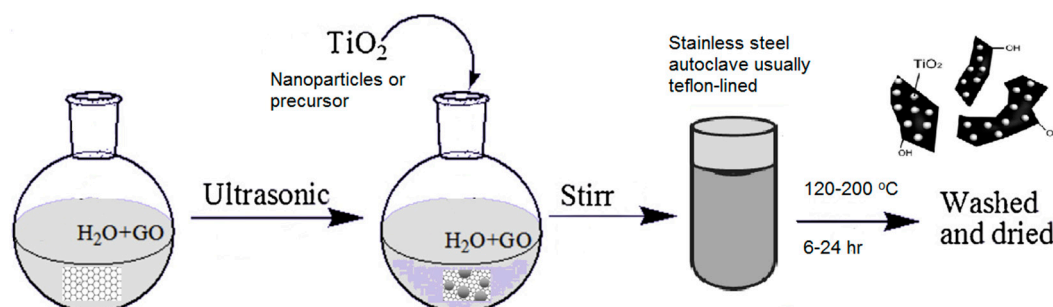


Figure 5. Schematic diagram of the HT synthesis of TiO_2/G nanocomposites, adapted with permission from reference [90]. Copyright 2014 Elsevier.

The HT method uses TiO_2 nanoparticles or nanowires as the source of TiO_2 [91,92]. Other TiO_2 precursors, such as TiCl_4 , TiF_4 , titanium nitride (TiN), $(\text{NH}_4)_2\text{TiF}_6$, tetrabutyl-titanate (TBT) or Ti (IV) isopropoxide, to produce TiO_2 nanoparticles are other alternatives to produce TiO_2/G and TiO_2/GO nanocomposites [93]. TiCl_4 and GO were used in one-step HT synthesis of TiO_2/G as the reduction of GO to G and the hydrolysis of TiCl_4 to TiO_2 nanoparticles were attained simultaneously. The formed TiO_2 nanoparticles were bi-phasic; including both anatase and rutile phases. FTIR characterization confirmed the incomplete reduction of GO. The effect of different GO amounts in the formed nanocomposites was studied with the composite of 2 wt% GO showing the best photocatalytic activity in the degradation of rhodamine B dye. The presence of reduced GO in the formed TiO_2/G nanocomposites improved the photocatalytic activity by increasing the surface area, as confirmed using N_2 Desorption Isotherms, giving more active sites, and producing more reactive species [89]. Similar results were reported by Li using different amounts of commercial TiO_2 (P25) in aqueous dispersions of GO, followed by heating at 120 °C for 3 h in absence of reducing agents. The results showed that increasing the amount of G in the formed TiO_2/G nanocomposites is accompanied by an increase in the surface area and the adsorption capacity for dyes [94]. Uniform TiO_2 nanoparticles distribution on the surface of G sheets was successfully achieved by Bai using the HT technique [93]. TiF_4 was used as a TiO_2 precursor, HI was used as a reducing agent for GO and morphology controlling agent. Scanning Electron Microscopy (SEM), Transmission Electron Microscopy (TEM), FTIR and Raman spectroscopy were used to confirm the results. The formed TiO_2/G nanocomposites showed high stability under both visible ($\lambda = 400 \text{ nm}$) and UV ($\lambda = 365 \text{ nm}$) light irradiation. The improved photocatalytic activity of TiO_2/G nanocomposites compared to bare TiO_2 was ascribed to the reduction in the electron-hole recombination rate in the formed nanocomposites. The effect of the medium pH on the photocatalytic activity of the formed nanocomposites was studied and found that increasing the pH value resulted in an increase in the photocatalytic degradation of bisphenol A (BPA). Optimum

degradation of BPA was at pH 11, where alkaline medium induces the production of more HO[•] and improves the photocatalytic activity [93].

Nitrogen-doped anatase and G were used to synthesize N-doped TiO₂/G nanocomposites with enhanced photocatalytic activity by the HT method. The TiN solid powder served as the precursor of the N-doped TiO₂ nanoparticles and GO was partially reduced during the HT reaction [95]. Gu reported the HT preparation of N-doped, N and V co-doped TiO₂/G and TiO₂/GO nanocomposites with higher visible light photocatalytic activity than bare TiO₂ under visible light irradiation [90]. Amine-functionalized TiO₂ nanoparticles with surface positive charges improved the interaction with GO sheets with surface negative charges. The wrapping of TiO₂ with G and partial reduction of GO were achieved during the HT reaction [96,97]. Furthermore, amine-functionalized TiO₂ nanoparticles, were used to prepare recyclable magnetic TiO₂/G nanocomposites using magnetic Fe₃O₄ nanoparticles coating silica substrates. The recyclable magnetic TiO₂/G nanocomposites showed improved photocatalytic activity, due to the presence of G which acted as an electron sink for the photoinduced electrons. Nanocomposite recovery was achieved using a magnetic field [98].

The HT method was used by Ariffin to produce a photocatalytic filtration system for water treatment applications. TiO₂/G nanocomposites were deposited on a polypropylene porous filter. Titanium (IV) isopropoxide, as a TiO₂ precursor, in triethanolamine (TEA) was added to GO suspension in aqueous ethanol and stirred at room temperature. It was then placed in contact with the polypropylene porous filter and heated to 120 °C for 24 h. The polypropylene filter thus modified with TiO₂/G exhibited high mechanical stability and improved photocatalytic activity, as measured by photodegradation of methylene blue and repeated for five cycles, as compared with the filter with TiO₂ only [99].

Nguyen investigated the effect of temperature variation on the surface area and crystal phase during the HT synthesis of TiO₂/G flower-like nanocomposites. The results showed that lower temperatures resulted in amorphous samples with larger surface area. On the other hand, higher temperatures resulted in the formation of the TiO₂ anatase crystalline phase with lower surface areas for the prepared nanocomposites. This conclusion was based on the results of x-ray diffraction (XRD), SEM, nitrogen adsorption, and Raman spectroscopy [100]. Flower-like TiO₂/G nanocomposites can be prepared using dropwise addition of acetic acid. The flower-like configuration improved the photodegradation of rhodamine B and trichloroethylene which was ascribed to the large increase in the surface area [101]. Furthermore, Zhang reported the importance of calcination of the hydrothermally prepared TiO₂/G nanocomposites to restore some surface oxygenated functional groups and improve TiO₂ crystallinity. Calcined samples showed better photocatalytic activity in degradation of methyl orange dye and disinfection of *E. coli*, compared to uncalcined TiO₂/G nanocomposites [102].

Facile, one-step HT reaction was used to prepare a TiO₂/G nanocomposites hydrogel with three-dimensional hierarchical inter-connected channels by Zhang. Compared with TiO₂, the prepared hydrogel showed increased activity as a photocatalyst, as a dye-adsorbent, and as a supercapacitor. This was attributed to improved photocatalytic activity, enhanced adsorption capacity, and increased electrochemical capacitive performance [103]. Ascorbic acid can be used as reducing agent and crosslinker in the formation of three-dimensional TiO₂/G aerogels with high stability, recyclability, and improved photocatalytic activity, as reported by Li [104] recently, TiO₂/G nanocomposite foams were prepared using TBT and G foams in an HT process. The prepared foams exhibited larger surface area, photocatalytic activity and light absorption than TiO₂ nanorods, as reported by Men [105].

An alkaline HT process, using NaOH, was used to transform commercial TiO₂ (P90) to TiO₂ nanotubes, and simultaneously reduce GO to G, giving TiO₂ nanotube-G nanocomposites [91]. The same approach was used by Pan to obtain TiO₂ nanowires-G nanocomposites. Aqueous solutions of KOH and commercial TiO₂ (P25) were heated at 200 °C for 24 h. The produced TiO₂ nanowires were added to GO aqueous suspension, and the mixture heated at 120 °C for 3 h. The TiO₂ nanowires were more uniformly distributed on the G surface, with less aggregation than TiO₂ nanoparticles, leading to

improved adsorption and photocatalytic activity [106]. Similar results were recently reported by other research groups [107,108].

The effect of glycerol during the HT synthesis of nanocomposites was studied by Shao. Glycerol inhibited the growth and agglomeration of TiO_2 in the solution and prevented the stacking of G sheets producing ultrafine TiO_2 nanoparticles of ca. 4 nm diameter homogeneously distributed on the G surface. This resulted in a large surface area, efficient charge separation, and high photocatalytic activity, towards rhodamine B and methylene blue degradation, for TiO_2/G nanocomposites prepared in the presence of glycerol [109].

Recently, graphene quantum dots (GQDs) were introduced as an excellent electron transfer agent that can improve the photocatalytic activity of TiO_2 effectively. Qu used the HT method to prepare TiO_2 nanotubes/GQDs nanocomposites with superior photocatalytic activity towards dye degradation, as methyl orange. The photocatalytic enhancement by GQDs was ascribed to three factors: efficient light absorption, improved photogenerated electron-pair separation, and photosensitization properties of GQDs [110]. TiO_2/GQDs nanocomposites exhibited superior photocatalytic activity in hydrogen evolution and photodegradation of dyes [111,112]. N-doped GQDs/ TiO_2 nanocomposites were prepared hydrothermally using ethylenediamine and citric acid as N and C precursors. The prepared N-doped GQDs/ TiO_2 nanocomposites showed excellent photocatalytic activity in the photocatalytic degradation of MB dye under UV light illumination [113]. N,S co-doped GQDs/G/ TiO_2 nanocomposites were prepared by alkaline HT process and improved the photocatalytic degradation of methyl orange dye under visible light illumination [114].

2.2. The Solvothermal (ST) Method

Akin to the definition given in Section 2.1, the term solvothermal synthesis refers to a method for growing crystals from a non-aqueous solution using an autoclave at high temperature and pressure. As shown in Figure 6, The ST method of synthesis is similar to the HT counterpart, except that non-aqueous solvents are employed to yield the TiO_2/G nanocomposites. The ST method usually provides better control over the size distribution, shape and crystallinity of the prepared nanomaterials compared to the HT method, probably due to a combination of the solvent properties such as viscosity and polarity (relative to those of water) and higher temperatures used [86].

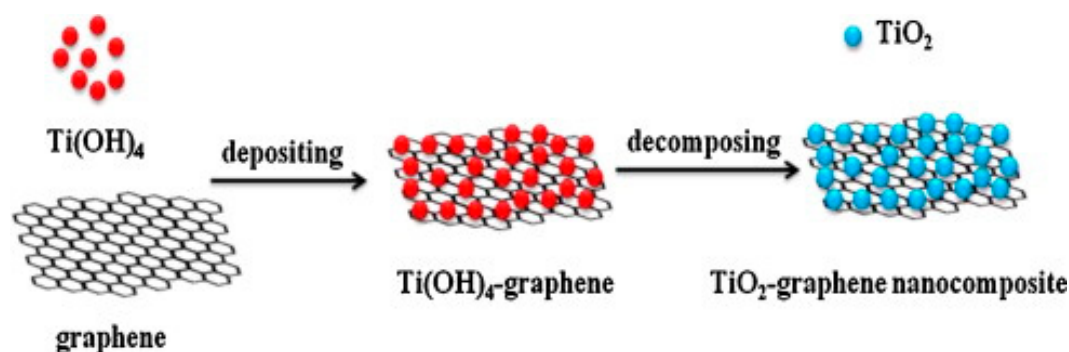


Figure 6. A schematic representation of the ST-based synthesis of TiO_2/G nanocomposites. Reprinted with permission from reference [115]. Copyright 2012 Elsevier.

Wang used a one-step ST method for the synthesis of G/CNTs (carbon nanotubes)/ TiO_2 composites. They mixed GO, multi-wall carbon nanotubes (MWCNTs) and tetrabutyl titanate (TBT), as a TiO_2 precursor, in 2-propanol. The photodegradation of methylene blue dye and photo-reduction of Cr(VI) under UV light illumination were doubled compared to TiO_2/G nanocomposites. The photocatalytic activity of the prepared nanocomposites was dependent on the CNTs content, with 5 wt% CNTs as the optimal mass ratio. The addition of CNTs improved the photocatalytic efficiency by increasing the rate of HO^\bullet formation, as confirmed using the fluorescence intensity of 2-hydroxyterephthalic acid [116].

In a study by Qian, N-doped TiO₂/G nanocomposites were prepared by heating a mixture of TBT, G, ammonium hydroxide in 2-propanol to 180 °C. Density functional theory (DFT) calculations were employed to explain the improvement in the photocatalytic activity after adding G to the N-doped TiO₂. It was suggested that N-doping generates empty states in the band gap of TiO₂ that lie beneath the Fermi energy levels of G. These states become filled with electrons when N-doped TiO₂ is in contact with G, causing ascending shift in the energy of TiO₂ bands, relative to G. This band position across the TiO₂/graphene hetero-junction results in energetically more favorable transfer of the photoexcited electrons, leading to a better photocatalytic activity [117].

Li used two TiO₂ precursors, TiCl₄ and titanium (IV) isopropoxide, with GO. Pluronic P123, a triblock copolymer based on poly(ethylene glycol)-poly(propylene glycol)-poly(ethylene glycol) and a nonionic surfactant, was also used to prevent the agglomeration of TiO₂ nanoparticles and to increase the surface area of the prepared nanocomposites. This resulted in a sol that formed the required TiO₂/G nanocomposites upon ST treatment at 150 °C for 24 h. The formed nanocomposites exhibited high photocatalytic activity and stability under visible light and simulated sunlight illumination. This efficiency was ascribed to the improved textural properties, band gap narrowing and improved quantum efficiency of the produced nanocomposites [118].

Huang prepared chemically-bonded TiO₂/G nanocomposites prepared by dropwise addition of TBT ethanol solution to aqueous G dispersions containing known concentrations of G, followed by stirring and heating at 200 °C for 10 h. The resulting nanocomposites exhibited improved photocatalytic properties compared to the TiO₂/G nanocomposites prepared by mechanical mixing. The synergistic effect between TiO₂ and G through the formation of Ti–C chemical bonds increased the number of electron holes on the surface of TiO₂ and decreased the electron-hole pair recombination rates. This was confirmed by x-ray photoelectron spectroscopy (XPS) and photoluminescence (PL) spectroscopy [119].

Reduction of GO into G can be accomplished by adding glacial acetic acid during the ST process. Min added titanium (IV) isopropoxide to GO dispersion in acetic acid/ethanol solution. The mixture was stirred then heated at 120 °C for 24 h. The reduction of GO and deposition of TiO₂ onto G nanosheets were achieved during the ST process. The prepared TiO₂/G nanocomposites exhibited high photocatalytic activity under visible light illumination due to the formation of Ti–C and Ti–O–C chemical bonds at the hetero-junction as confirmed by XPS [120].

The morphology and shape of the formed TiO₂/G nanocomposites can be controlled using ethylene glycol as reported by Cai. Graphene nanosheets were sonicated with a TiCl₄ solution in this diol, and the mixture was heated at 180 °C for 12 h. The electrochemical behavior of the formed nanocomposites was investigated using coin-type cells against metallic lithium. High specific charge capacity was achieved, and the formed nanocomposites exhibited improved electrochemical performance [115]. Xie used glucose as a morphology controlling agent after addition to titanium (IV) isopropoxide/GO mixture in 2-propanol followed by H₂ reduction. The results showed that low glucose content can bridge chemically, through the surface hydroxyl groups, between GO surface and TiO₂ nanoparticles thus, results in well-dispersed TiO₂/G nanocomposites [121].

The morphology and shape of the prepared nanocomposites can also be controlled using HF as reported by Gu who synthesized TiO₂/G nanocomposites with exposed {001} facets through a one-step ST process. The nanocomposites were synthesized by adding TBT to GO suspension in 2-propanol followed by stirring. HF was added, followed by heating the mixture at 180 °C for 12 h. The trapping test, using ethylenediaminetetraacetic (EDTA) acid disodium salt as hole scavenger and *tert*-butanol as a radical scavenger, showed that the improvement in the photocatalytic activity was attributed mainly to the photogenerated holes in TiO₂ surface rather than the electrons transferred to G sheets [122].

2.3. Mechanical Mixing

This strategy is gaining attention due to its relative simplicity and the facile control of the reaction conditions. This method involves mixing dispersions of TiO₂ (either pristine or functionalized) and G or GO, possibly followed by sonication and stirring to provide maximum contact between

the nanocomposite starting materials [123], as illustrated in Figure 7. Gao prepared TiO₂/GO nanocomposites by mixing TiO₂ nanoparticles with GO dispersion in water, sonicating and stirring, followed by centrifugation and vacuum drying to produce the TiO₂/GO nanocomposites. The improvement in the photocatalytic activity was ascribed to the increase in the light absorption ability and effective electron-hole charge separation after mixing [124].

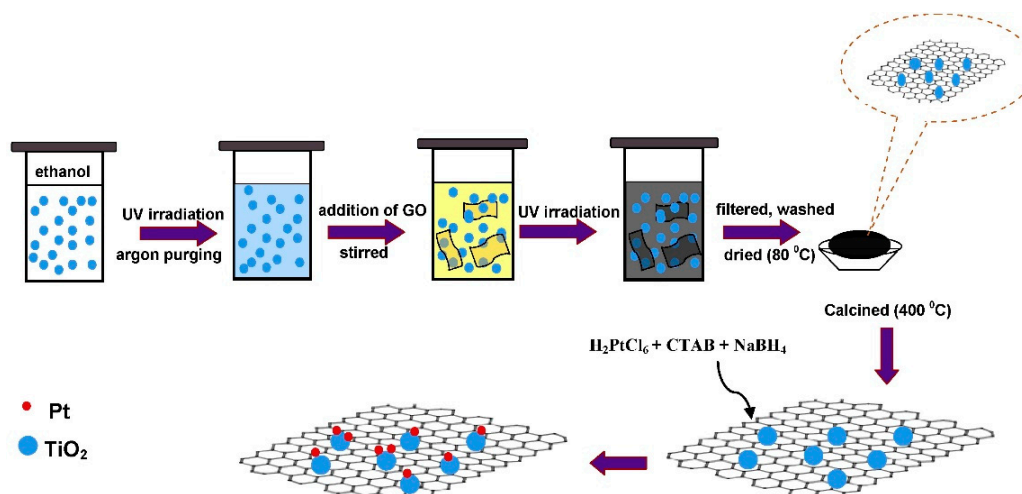


Figure 7. Schematic representation of the synthesis of TiO₂/GO nanocomposites by mechanical mixing and sonication. Reprinted with permission from reference [17]. Copyright 2013 Elsevier.

Large-scale production of TiO₂/GO nanorod composites (NRCs) was achieved by Liu using a two-phase system: GO dispersion in water and TiO₂ nanorods dispersed in toluene. The oleic acid (dispersant)-capped TiO₂ nanorods were synthesized by mixing *tert*-butylamine in water and titanium (IV) isopropoxide in oleic acid, followed by heating at 180 °C for 6 h. These nanorods were then added to GO aqueous dispersion with stirring at room temperature to ensure efficient co-ordination between GO and TiO₂ nanorods (no sonication employed). The prepared TiO₂/GO NRCs exhibited improved photocatalytic degradation of dyes and antibacterial activity compared to bare TiO₂ nanorods and TiO₂/GO nanoparticle composites, ascribed to the availability of more {101} facets and the effective electron-hole charge separation [125].

TiO₂/GO nanocomposites were synthesized by mixing in water, followed by sonication for 90 min. The photocatalytic activity of these nanocomposites increased as a function of increasing the GO content up to 10 wt% [126], in accordance with other reported results [94]. Thermal exfoliation of GO followed by treatment with nitric and sulfuric acids under sonication, was used to prepare carboxy-functionalized G. The as-prepared carboxy-functionalized G was added to the TiO₂ nanoparticles surface, as confirmed by FTIR, XRD, SEM, TEM, and Raman spectroscopy. The higher photocatalytic activity was attributed to the improved attachment of TiO₂ on the functionalized surface of the G sheets [127].

The reduction of GO to G can be achieved using UV light irradiation, heat, or chemical reducing agents during the synthesis process. Ghasemi prepared TiO₂/G nanocomposites by the simple mixing of TiO₂ and GO suspensions with sonication followed by the reduction of GO to G using UV light irradiation. The reduction of GO to G and the formation of Ti–C bonds were confirmed by XPS. The TiO₂/G nanocomposites were then doped with Pt and Pd and the Pt–TiO₂–G nanocomposites showed the highest photocatalytic activity [17]. These results were corroborated with recent work conducted by Shengyan [128]. UV irradiation was also used to reduce GO to G in the synthesis of G-coated TiO₂ nanocomposites. These led to an increase in photocatalytic hydrogen production, and photo-current generation, which was ascribed to the favorable interfacial charge transfer between TiO₂ and G nanosheets [129]. The same reduction procedure was used to produce

TiO₂/G nanocomposite films by drop- and spin-casting onto fluorinated tin-oxide slides. The films exhibited better electron lifespan and improved photocurrent generation [130].

Thermal treatment of TiO₂/GO composites under inert atmosphere was reported to partially reduce the surface oxygenated groups of GO resulting in TiO₂/G nanocomposites with improved photocatalytic activity. The results showed that the charge separation in the TiO₂/G nanocomposites is more efficient relative to the TiO₂/GO nanocomposites. Additionally, increasing the GO content beyond 1.4 wt% reduced the photocatalytic performance, similar results were reported by Zhang [71,123].

2.4. Sol-Gel Methods

Sol-gel methods involve the synthesis of inorganic ceramics from solution by transforming the liquid precursor to a *sol* that gradually develops into a *gel* network structure [131]. The sol is a colloidal suspension that is formed by hydrolysis and condensation of the metal-alkoxide precursor. Sol-gel methods for TiO₂-based nanocomposites involve the hydrolysis of an appropriate TiO₂ precursor, usually a Ti alkoxide, followed by condensation in the presence of G or GO. An important advantage of sol-gel methods is the fact that elevated temperatures and pressures are not needed. Other advantages include reliability, controllability and low cost are reflected in sol-gel preparation of TiO₂/G nanocomposites [132]. The formation of Ti–O–C and Ti–O–Ti bonds is favored with low hydrolysis rate, low quantities of water, and the presence of excess Ti precursor [16,86]. The addition of TiO₂ precursors to the GO dispersions leads to the formation of relatively stable oxo- and hydroxo-bonds between TiO₂ and G surfaces leading to the formation of sols, then of gel-like network structures with the addition of more GO. These structures produce the desired nanocomposites upon drying and/or calcination as shown in Figure 8.

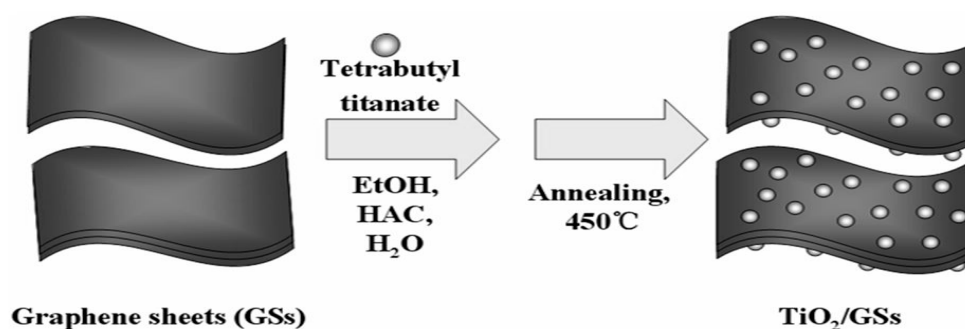
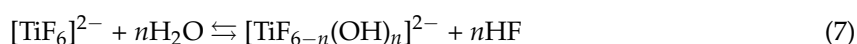


Figure 8. Schematic diagram of the sol-gel preparation of TiO₂/GO nanocomposites. Reprinted with permission from reference [133]. Copyright 2010 Royal Society of Chemistry.

Štengl used TiO₂ peroxy-complexes as a precursor to prepare TiO₂/GO nanocomposites with varying GO contents using a one-step sol-gel method. NaOH and hydrogen peroxide were used to hydrolyze titanium oxysulfate (TiOSO₄) and produce a TiO₂ peroxy-complex [16]. In order to prepare TiO₂/G nanocomposites, Liu used titanium (IV) isopropoxide as the TiO₂ precursor, and reduced GO into G using hydrazine hydrate. The nanocomposites were formed by the dropwise addition of the Ti precursor into a mixture of G and the cationic surfactant cetyltrimethylammonium bromide in ethanol under stirring. Water was added to the mixture, and the suspension was stirred, dried and annealed at 500 °C for 5 min [134]. Titanium oxysulfate was used as a TiO₂ precursor by Park in a sol-gel process to prepare CdS-G-TiO₂ nanocomposites with improved photocatalytic activity under visible light illumination. The nanocomposites were synthesized by adding titanium oxysulfate precursor to CdS-G composites, previously prepared by mixing CdCl₂, Na₂S and GO, followed by drying and heating at 500 °C. CdS improved the photocatalytic degradation of methylene blue under visible light illumination, due to bandgap narrowing and enhanced visible light absorption [135].

2.5. Depositions Techniques: Liquid Phase Deposition (LPD), Aerosol Deposition (AD), Chemical Vapor Deposition (CVD), and Electrospinning

These techniques share the advantages of simplicity of the experimental procedure and formation of the nanocomposites at relatively low temperatures. The term liquid phase deposition, LPD, refers to the slow hydrolysis of a metal–fluoro complex $[\text{MF}_n]^{m-n}$ from an aqueous solution by addition of water to produce thin oxide films. Complexing agents are used to collect the liberated fluoride ions, e.g., boric acid or aluminum metal.



While the addition of water causes the precipitation of the oxide, aluminum and boric acid act as fluoride scavengers that destabilize the fluoro complex and affect the oxide precipitation [136].

Pastrana-Martínez used LPD to deposit TiO_2 on the surface of G nanosheets using ammonium hexafluorotitanate (IV), $(\text{NH}_4)_2\text{TiF}_6$, as the TiO_2 precursor and G sheets produced by thermal reduction of GO. The hydrolysis of the TiO_2 precursor and the production of the TiO_2/G nanocomposites stabilized by hydrogen-bonds occur simultaneously [137,138]. Similarly, Jiang used $(\text{NH}_4)_2\text{TiF}_6$ and G, prepared by thermal reduction of GO, to prepare TiO_2/G nanocomposites by LPD. The prepared nanocomposites have enhanced photocatalytic activity ascribed to improved adsorption capacity, electron transfer and larger surface area [139]. Recent work by Zhang used LPD and the same precursor, $(\text{NH}_4)_2\text{TiF}_6$, to prepare sandwich-like TiO_2/G nanocomposites with enhanced photocatalytic activity due to unique morphology with a consequent increase in surface area and photocatalytic activity [140].

Ultrafiltration membranes were prepared using LPD methods. The prepared membranes combine the photocatalytic degradation activity of TiO_2/G nanocomposites with the membrane filtration capacity. Athanasekou used the dip-coating process for the deposition of TiO_2/GO nanocomposites on the surface of ceramic membranes. These membranes included γ -alumina and silica single channel nanofiltration membranes with a pore size from 1 to 10 nm. The performance of the hybrid photocatalytic/ultrafiltration system exhibited improved pollutant removal efficiency compared to the reference membrane prepared by the same dip-coating technique using TiO_2 without GO [18].

Antifouling hierarchical filtration membranes were prepared by filtering a dispersion of TiO_2/GO composite in ammonium hydroxide through polycarbonate filter membranes. This was followed by the deposition of a layer of TiO_2 with a strong photocatalysis activity. The filtration capacity and photocatalytic degradation of direct red 80 and direct blue 15 dye solutions under UV-light illumination of these membranes, showed that the antifouling effect improves the water treatment ability [141].

Another deposition variety that results in porous films is aerosol deposition (AD) in which a high-speed gas jet is used to force the precursor powder to form a colloidal aerosol. These accelerated particles collide with the substrate at high speed, forming a condensed film at room temperature. This approach offers the advantage of continuous, single-step operation to produce tunable film structures with corresponding functionalities [142–144]. An example of this experiment for producing TiO_2/G film is shown in Figures 9 and 10. First TiO_2/G powder was obtained by the scheme shown in Figure 9:

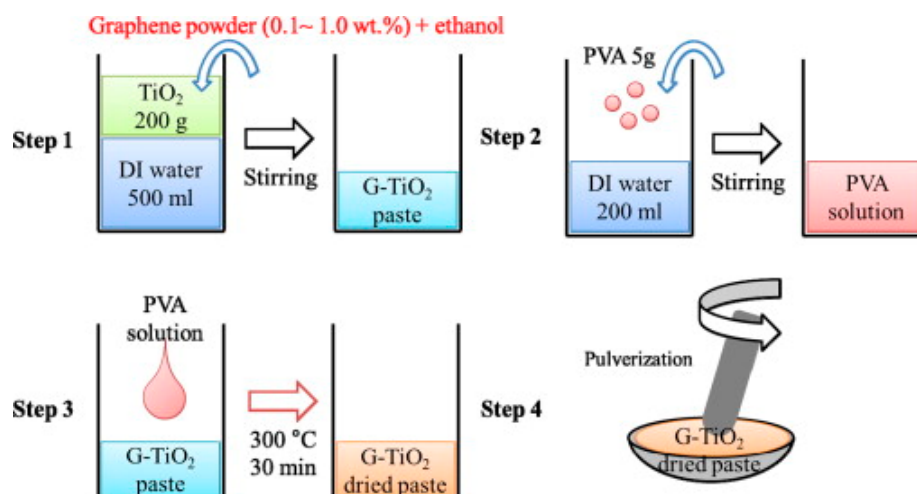


Figure 9. Scheme employed to prepare TiO₂/G powder for the AD experiment. Reprinted with permission from reference [144]. Copyright 2014 Elsevier.

The obtained powder is then shaped into a film using the setup shown in Figure 10.

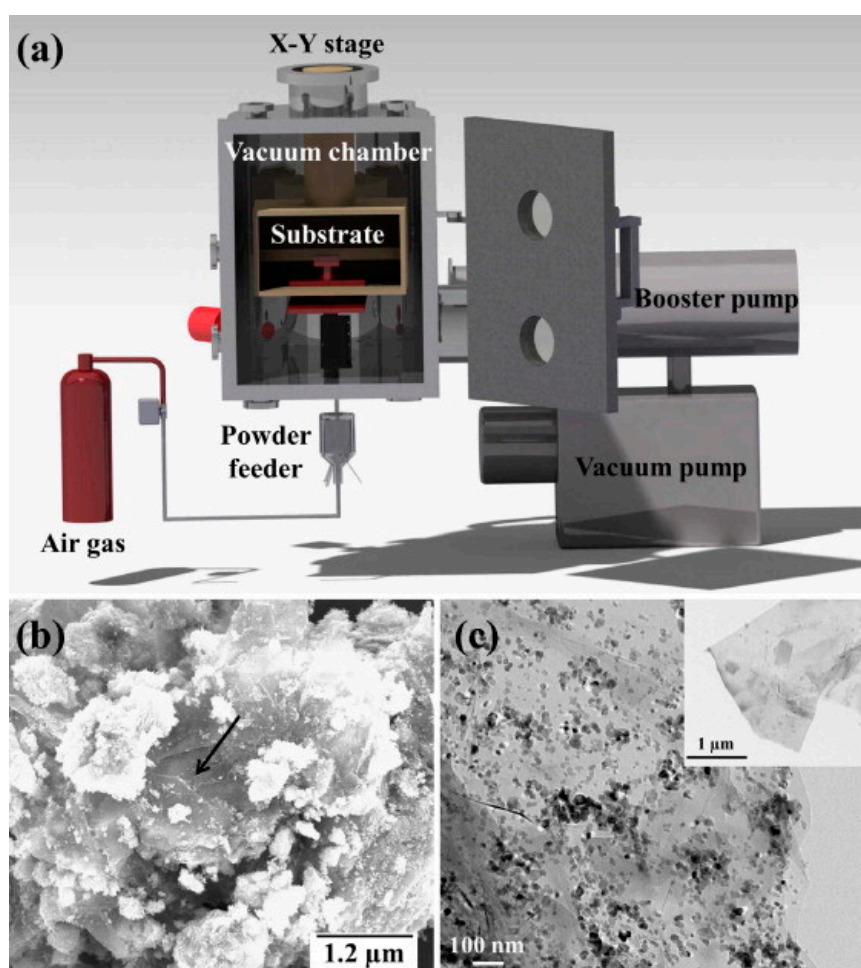


Figure 10. Schematic diagram of the AD experiment and the results obtained. Part (a) shows the air gas tank, powder feeder, nozzle, vacuum chamber, and pumps, parts (b) and (c) show the SEM and TEM images of the TiO₂/G nanocomposite. Reprinted with permission from reference [144]. Copyright 2014 Elsevier.

Qin used a combination of techniques to prepare multilayer composites of G and TiO₂. A large-scale monolayer graphene film was synthesized by CVD on Cu foil deposited on SiO₂ wafer, by passing CH₄/H₂ mixture at 1000 °C, followed by cooling. A polymer support, poly(methyl methacrylate)(PMMA), was attached to the G film by spin-coating. The Cu and polymer layers were subsequently removed by treatments with ammonium persulfate (Cu) solution and acetone (PMMA), to yield G/SiO₂ chip. TiO₂ was deposited on this chip by AD to give G/TiO₂/SiO₂ chip, and the steps repeated to get G/TiO₂/G/SiO₂. The photocurrent performance of the formed nanocomposites was measured and evaluated for future applications in the production of photoelectric devices [145].

Wojtoniszak used CVD to prepare TiO₂/G nanocomposites with improved photocatalytic activity. TiO₂/G nanocomposites were prepared by adding pristine TiO₂ in a horizontal furnace with a quartz tube reactor. Acetylene was the carbon source for G and was heated at 400–500 °C in the presence of TiO₂. Higher production temperature and shorter CVD time led to the highest photocatalytic degradation activity among the prepared samples [146]. Gao used layer by layer (LBL) deposition for the preparation of a photocatalytic TiO₂/GO grafted filter membrane. They poured a TiO₂ suspension followed by a GO dispersion onto a polysulfone base membrane to obtain the composite membrane. The reduction of GO to G was achieved by UV irradiation. The efficiency of the LBL process in depositing TiO₂/GO onto the membrane was determined by the quartz crystal microbalance. The TiO₂/GO membranes showed improved photocatalytic activity under UV and simulated sunlight illumination [147].

Microwave-assisted one-step synthesis of TiO₂/G nanocomposites was reported by Yang. In this approach, the reduction of GO to G and the coating of TiO₂ on the G nanosheets occur concurrently. The TiO₂/G nanocomposites were produced by mixing a GO dispersion in water with commercial TiO₂ (P25), and the mixture was heated in a microwave equipment at 140 °C for 5 min. The TiO₂/G nanocomposites showed increased photocatalytic activity due to improved charge separation, light absorption, and dye adsorption capacity of the prepared nanocomposites [148]. A similar approach was used by Shanmugam to prepare TiO₂/G nanocomposites that exhibited almost 10-fold increase in the BET surface area compared to TiO₂ nanoparticles with an increase in the photocatalytic degradation activity under both UV and visible light illumination [149].

Self-cleaning applications of TiO₂/G nanocomposites were investigated by Anandan after preparing the TiO₂/G nanocomposites using spin-coating technique. They used titanium (IV) bis-ammonium lactate dihydroxide together with G sheets in the presence of glycerol to produce a homogeneous ceramic film on a glass substrate, which was calcinated at 400 °C before use. The prepared structure exhibited enhanced photoactivity and superhydrophilicity under UV light illumination [19].

Electro-spinning was used to prepare TiO₂/G nanocomposites with enhanced photocatalytic and photovoltaic properties. The TiO₂/G nanocomposites were prepared by dispersing G in *N,N*-dimethylacetamide containing polyvinyl acetate (PVAc) and TiO₂. This was followed by electrospinning and sintering at 450 °C for 1 h. The prepared TiO₂/G nanocomposites exhibited enhanced photocatalytic and photovoltaic properties, as compared with TiO₂ nanoparticles, for the photodegradation of azo dyes, and for use in dye-sensitized solar cells [150].

3. Characterization of TiO₂/G and TiO₂/GO Nanocomposites

The properties of TiO₂/G and TiO₂/GO nanocomposites, as well as their photocatalytic applications, depend mainly on the structure, morphology and the surface properties of the prepared nanocomposites. Therefore, various characterization techniques are employed for the characterization of TiO₂/G and TiO₂/GO nanocomposites used for photocatalytic applications. The most relevant of these techniques are reviewed below, using representative examples.

3.1. Structural and Elemental Analysis

3.1.1. X-ray Diffraction (XRD)

XRD is used for providing information about the crystal phase structure and phase purity of crystalline materials. In addition, the average particle size is calculated from the broadening of the appropriate peak in the XRD spectrum using Scherrer's equation:

$$D = K\lambda / \beta \cos\theta \quad (9)$$

where, K is a dimensionless factor with a value close to unity, λ is the wavelength in Angströms (\AA), β is the width at half height of the respective XRD peak, θ is Bragg's angle and D is the mean particle diameter in (\AA).

Although XRD is widely used for structure determination of nanomaterials, it is of little use for amorphous materials as this technique requires highly ordered crystal lattice structure in order to provide useful information. In addition, mixtures of phases with low or no symmetry will produce a large number of diffraction points causing a poor differentiation between the multiple phases [151].

Bai used XRD to confirm that the formation process of TiO_2/G nanocomposites had no significant effect on the crystal phase of anatase. Additionally, the reduction of GO to G was confirmed by the disappearance of the GO peak at $2\theta = 13\text{--}14^\circ$, and the presence of a peak at $2\theta = 26.5^\circ$ indicated that the stacking of G sheets is minimal as shown in Figure 11 [93]. However, the G peak at $2\theta = 26.5^\circ$ could typically be masked in the TiO_2/G nanocomposites due to strong peak at $2\theta = 25.2^\circ$ which is attributed to the anatase phase of TiO_2 [127,148].

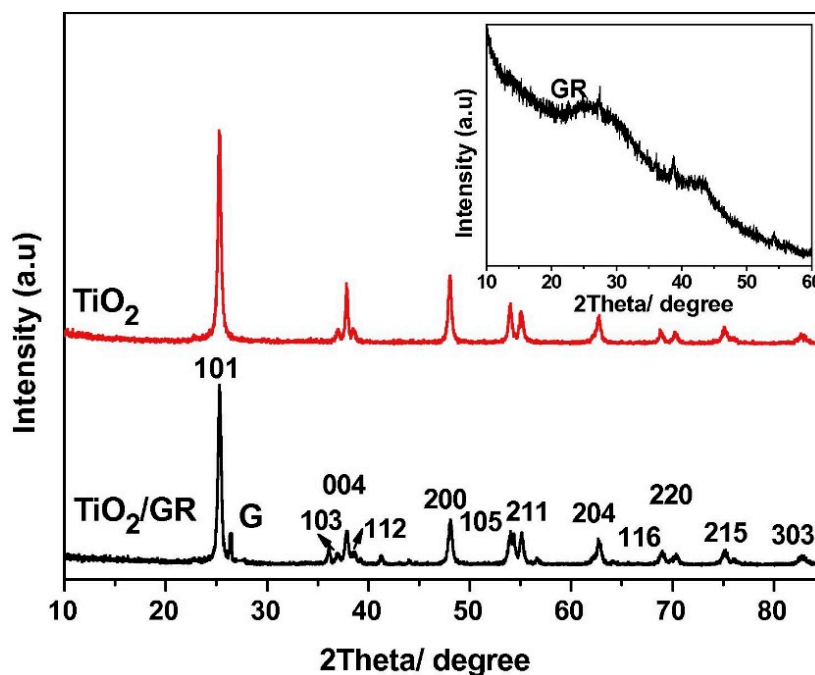


Figure 11. XRD diffractogram of TiO_2 , $\text{TiO}_2/\text{reduced G (GR)}$ nanocomposites and bare GR (inset). Reprinted with permission from reference [93]. Copyright 2014 Elsevier.

3.1.2. Energy Dispersive X-ray Analysis (EDX)

EDX is used for the elemental analysis of different nanocomposites, see Figure 12. Hence it provides information about the ratio of the elements at the surface of the nanocomposite. However, poor resolution and spectral overlapping make EDX unreliable for quantitative analysis of elements [127]. Park used EDX to confirm the formation of Ti–C bonds in $\text{CdS-G}/\text{TiO}_2$ nanocomposite due to the formation of surface complexes that include carbon atoms and TiO_2 . These surface complexes

were increased after treating the surface of the nanocomposites with nitric acid which improved the uniformity and homogeneity of TiO_2 distribution onto G sheets [135]. The O/Ti atom percentage using EDX was used to confirm the partial reduction of GO to G in accordance with IR results [152].

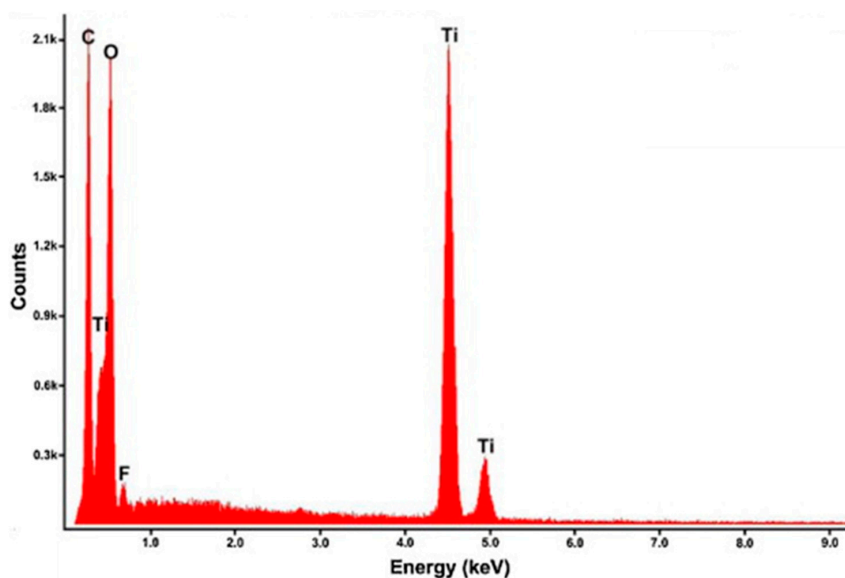


Figure 12. EDX spectrum of TiO_2/GO nanocomposite, showing the presence of C, O, and Ti elements. Reprinted with permission from reference [137]. Copyright 2012 Elsevier.

3.2. Size and Morphology Analysis

3.2.1. Scanning Electron Microscopy (SEM)

SEM is a very useful technique for the examination of nanoscale materials because the three-dimensional images provide better information about the sample as a result of the significant depth of focus of SEM [153]. Nguyen used SEM to confirm the formation of the nanocomposites between TiO_2 and G sheets. Field emission SEM was used to show better “flower-like” structure of the formed TiO_2/G nanocomposites prepared by HT method under 120°C . In addition, they reported the formation of nanoflakes on the surface of TiO_2/G nanocomposites with the increase in the preparation temperature. This was attributed to self-assembly of the nanorods and nanoflakes on the surface of the formed nanocomposites through van der Waals forces [100], as shown in Figures 13 and 14. Ni used SEM to confirm the wrapping of G on the TiO_2 nanoparticles. They reported that increasing the G load increases the wrapping of G nanosheets onto the TiO_2 surface. However, the excess G loading will decrease the photocatalytic activity of the prepared nanocomposites as G will interfere with the efficiency of light absorption by TiO_2 [97].

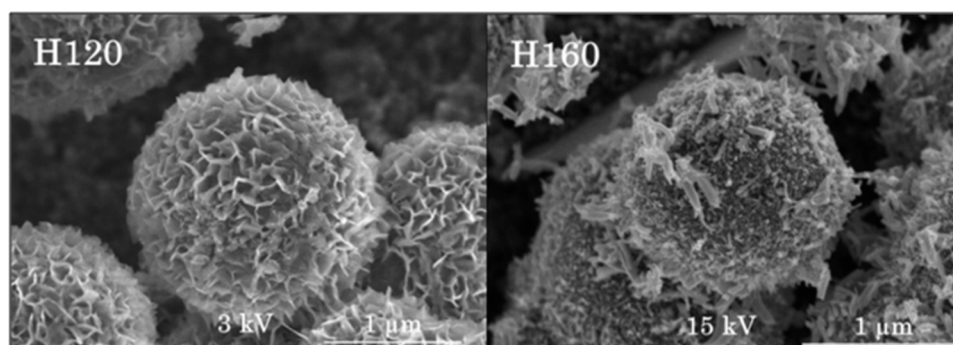


Figure 13. SEM images of TiO_2/G nanocomposites prepared by HT method at 120°C (H120) and 160°C (H160). Reprinted with permission from reference [100]. Copyright 2014 Elsevier.

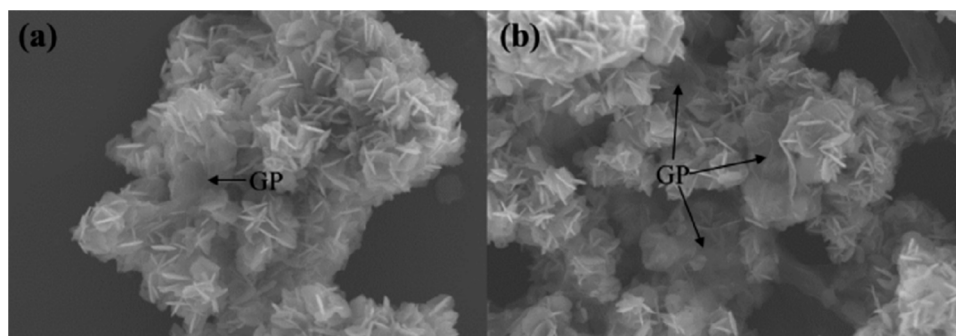


Figure 14. SEM images of TiO₂/GO nanocomposites with different G loadings using magnification $\times 10,000$. Reprinted with permission from reference [97]. Copyright 2014 Elsevier.

3.2.2. Transmission Electron Microscopy (TEM)

Useful information about the surface structure, interface between the nanocomposite components, particle size and morphology of TiO₂/G nanocomposites can be obtained using TEM [154,155]. Gao employed this technique to confirm the spherical shape of the TiO₂ nanoparticles with high photocatalytic degradation activity and the formation of TiO₂/G nanocomposites [124], whereas Xu showed that TiO₂ nanoparticles are spread sporadically on the surface of GO due to low loading amount of TiO₂. This partial covering result in restacking of GO sheets into hierarchical membranes with TiO₂ nanoparticles trapped within as shown in Figure 15. These membranes have potential use in water purification [141].

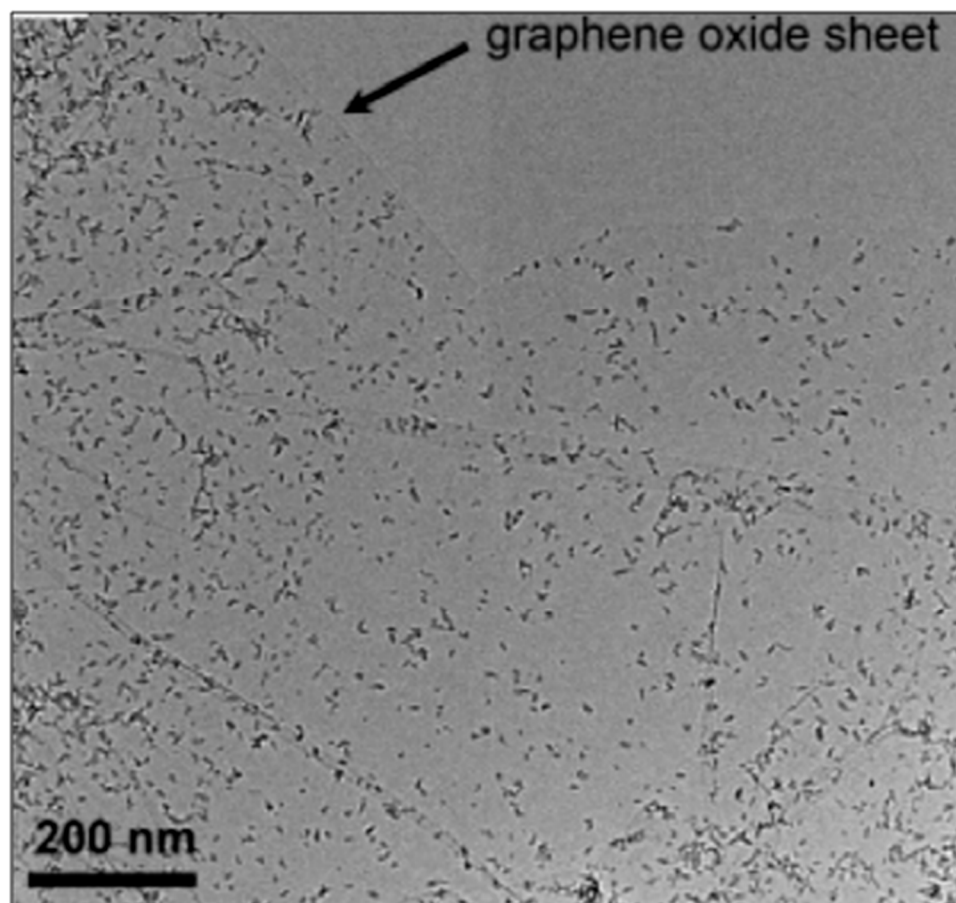


Figure 15. TEM image of TiO₂/GO nanocomposite with low TiO₂ loading. Reprinted with permission from reference [141]. Copyright 2014 American Chemical Society.

3.2.3. Atomic Force Microscopy (AFM)

AFM is used to study the electrical properties, morphology and surface interactions of nanocomposites, and to probe the surface structural features of the scanned materials. However, the use of AFM to study the topographical and morphological properties of TiO₂/G and TiO₂/GO nanocomposites is uncommon due to the limited scan area and the possible fast deformation of the probe tip [151]. Li used AFM images and the associated height profile to show that the fabricated G is a single layer and that the formed TiO₂/G nanocomposites contain the TiO₂ nanoparticles uniformly distributed on the surface of the G nanosheets [118]. Additionally, Ghasemi used AFM to show that the average height of the G sheets is 0.85 nm while the average height of the formed TiO₂/G nanocomposites is 2.72–3.82 nm [17], as shown in Figure 16. Formation of three layers of GO and the stacking of G layers during formation of the TiO₂/G nanocomposites was also confirmed using AFM [122].

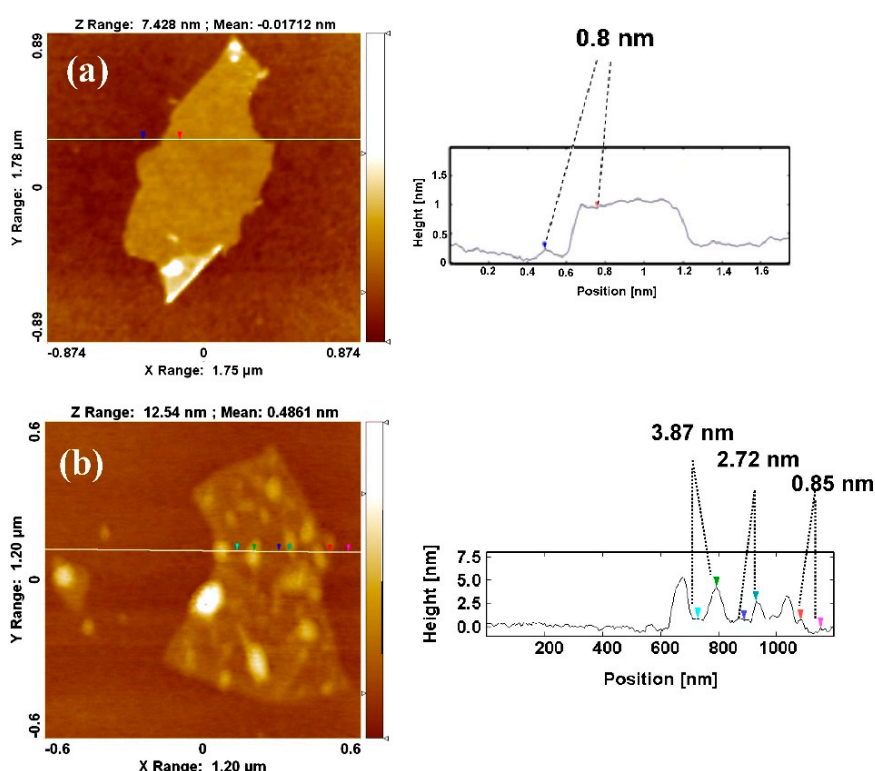


Figure 16. AFM images and height profiles of (a) GO and (b) TiO₂/G nanocomposites. Reprinted with permission from reference [17]. Copyright 2013 Elsevier.

3.3. Textural Analysis

Nitrogen Adsorption/Desorption Isotherms

Textural properties such as pore size distribution, pore volume, and specific surface area can be obtained using the nitrogen adsorption/desorption measurements. The surface area of the material examined (S_{BET}) is usually calculated using the Brunauer–Emmett–Teller (BET) equation:

$$S_{\text{BET}} = n A_m N \quad (10)$$

where, $n = V_m/22,414$ (V_m is the monolayer capacity), A_m is the molecular cross-sectional area occupied by the adsorbate monolayer per gram of adsorbent, and N is Avogadro's number [156,157]. The determination of S_{BET} is important because the applications for the formed nanocomposites are greatly affected by their surface areas. Shi used the N₂ adsorption-desorption isotherms to

demonstrate the presence of mesopores and macropores in the prepared TiO₂/G nanocomposites. They demonstrated that the specific surface area of the latter is larger than that of TiO₂, with subsequent enhancement of the photocatalytic activity of the formed nanocomposites [95]. These findings are in agreement with the results of Yang who demonstrated an increase in the BET surface area, and the photocatalytic activity, with the increase in the G loading till 10 wt% in TiO₂/G nanocomposites [148]. The higher surface area of TiO₂/GO nanocomposites compared to their TiO₂/G counterparts are attributed to the better assembly of TiO₂ nanoparticles on the oxygenated surface of GO and better distribution of GO in the solution during the nanocomposite preparation [158]. On the other hand, increasing the HT treatment temperature during the formation of TiO₂/G nanocomposites decreases the BET surface area because of the increase in pore size. This is ascribed to the change in the morphology and crystal structure by forming nanoflakes rather than the flower-like crystals as a result of the increase in the HT temperature, with a subsequent decrease in the specific surface area of the nanocomposites, as shown in Figure 17 [100].

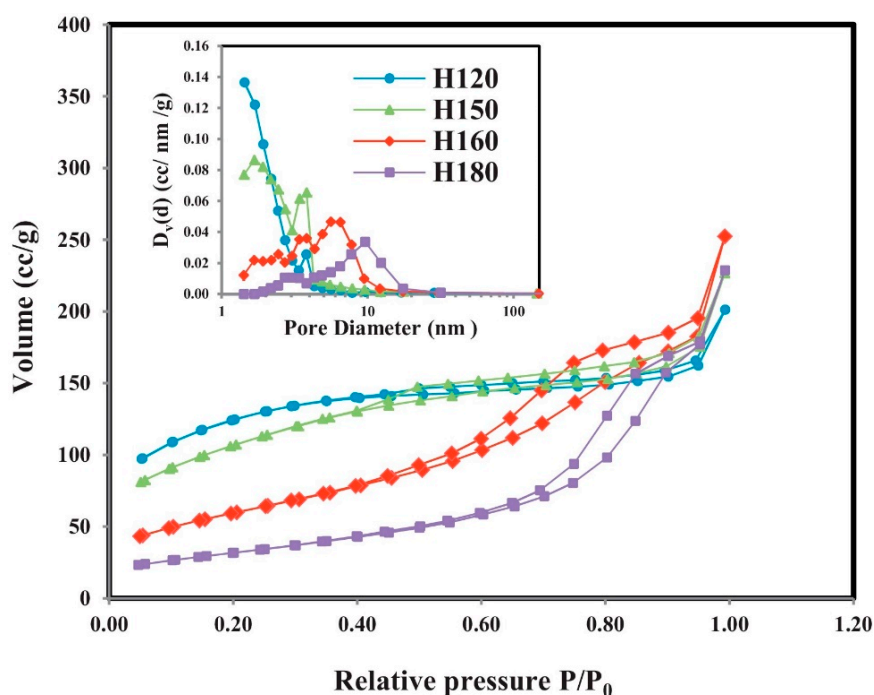


Figure 17. Nitrogen adsorption-desorption isotherms and pore size distribution (inset) of TiO₂/G nanocomposites prepared by HT at different temperatures. Reprinted with permission from reference [100]. Copyright 2014 Elsevier.

3.4. TiO₂ Band Gap Energy Analysis

The band gap energy analysis and the study of the recombination rate, between the photoinduced electrons and the photogenerated positive holes on the surface of the TiO₂ nanoparticles are crucial factors for the photocatalytic activity of TiO₂/G nanocomposites. The band gap narrowing and decreased recombination rate that is associated with the addition of G to TiO₂ nanoparticles can be calculated using different techniques, which are summarized hereafter [123].

3.4.1. UV-Visible (UV-Vis) Spectroscopy

UV-Vis Spectroscopy is the main technique used to measure the photocatalytic effect of TiO₂/G and TiO₂/GO nanocomposites on the degradation of environmental pollutants, such as polycyclic aromatic compounds and dyes. It was used to demonstrate the red shift in the absorption of N-doped TiO₂, relative to the undoped sample [117]. Yang and Pastrana-Martínez reported a redshift using TiO₂/G nanocomposites that results in narrowing the band gap and more efficient light harvesting

in the visible range. This redshift of ca. 50–60 nm was ascribed to the formation of Ti–O–C chemical bonds as reported for other carbon–TiO₂ nanocomposites [138,148].

On the other hand, diffuse reflectance UV–Vis spectroscopy (DRS–UV) is used to determine the band gap narrowing and the enhancement in visible light absorption. The sample reflectance is measured, converted into absorbance (using the Kubelka–Munk equation) [159], and the resultant spectrum is used to calculate the band gap energy between the conduction and valence bands of the formed TiO₂/G nanocomposites [119,158,160]. DRS–UV was also used to show that increasing the GO content in the TiO₂/GO nanocomposites increases light absorption in the visible region due to the increase in the availability of surface oxygenated groups that can react with the TiO₂ nanoparticles as shown in Figure 18 [123]. For TiO₂/G nanocomposites, an increase of the G content decreases the band gap energy, leading to a redshift and enhancement of the photocatalytic degradation of various environmental pollutants [94].

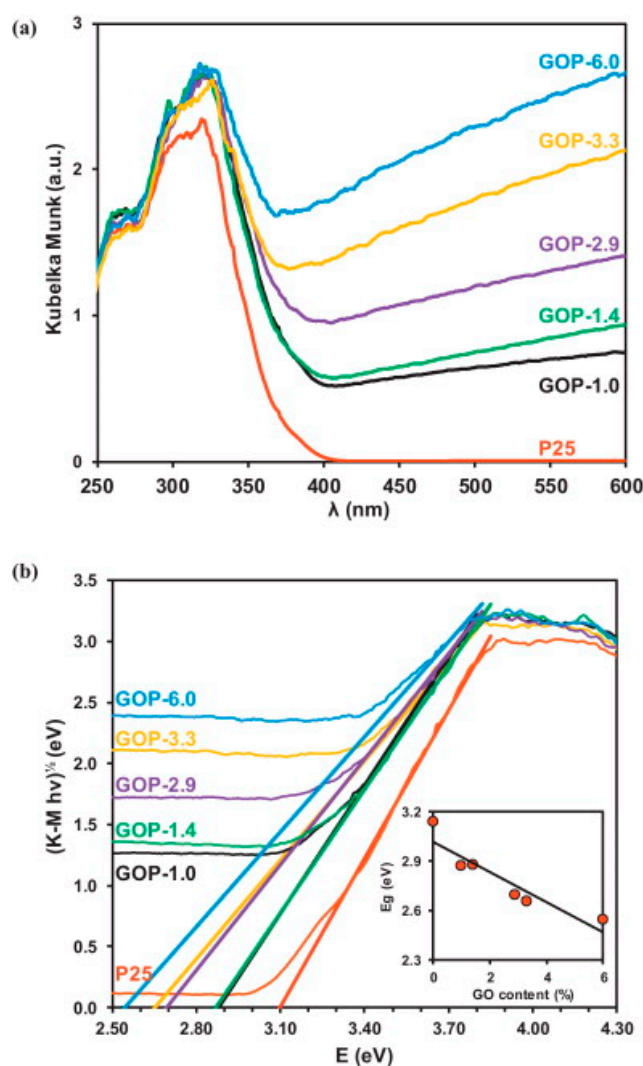


Figure 18. An example of the effect of the GO content on the UV–Vis absorption spectra (equivalent absorption Kubelka–Munk units) of TiO₂/GO nanocomposites, and calculated band gap (in eV). Part (a) shows the transformed spectra of bare TiO₂ (P25) and those of the synthesized nanocomposites as a function of increasing the GO content (1 to 6 wt%). Part (b) shows the relationship between the transformed Kubelka–Munk function and the energy of absorbed light. The effect of GO content on the band gap energy is shown in the inset. Reprinted with permission from reference [123]. Copyright 2013 Elsevier.

The effect of changing the preparation method of TiO₂/G nanocomposites on the band gap narrowing was studied by Fan using DRS-UV. The results showed that the sample prepared under HT conditions had the highest red shift and the largest band gap narrowing compared to the samples prepared by UV-assisted photoreduction, or by hydrazine chemical reduction. Furthermore, the effect of changing the mass ratio of TiO₂ to G was also studied by DRS-UV and the optimum ratio of TiO₂/G of 1/0.2 exhibited the highest photocatalytic activity [161]. The increased light absorption intensity of TiO₂/G nanocomposites compared to pure anatase TiO₂, resulted in an increase of the photocatalytic reduction of CO₂ under ambient conditions. This was supported by the decrease in band gap energy from 3.2 eV to 2.9 eV by the addition of G as measured by DRS-UV [162].

3.4.2. Electrochemical Impedance Spectroscopy (EIS)

EIS is used in the characterization of TiO₂/G and TiO₂/GO nanocomposites to measure the effect of the addition of G on the rate of the recombination between the photoinduced electrons and the positive holes generated on the surface of the TiO₂ nanoparticles. The addition of G to TiO₂ will give a smaller semicircle in the EIS plot indicating a decrease in the charge transfer resistance through the surface of the TiO₂/G nanocomposites, as presented in Figure 19. This effect is induced by the large surface area of G and its *sp*² network, which acts as electron transport medium from the conduction band of TiO₂ to G. Consequently, the presence of G in the nanocomposites will decrease the above-mentioned recombination rate. This leads to an increase in the lifetime of the charge carriers and improves the overall photodegradation process induced by the nanocomposites [90,93,119,163].

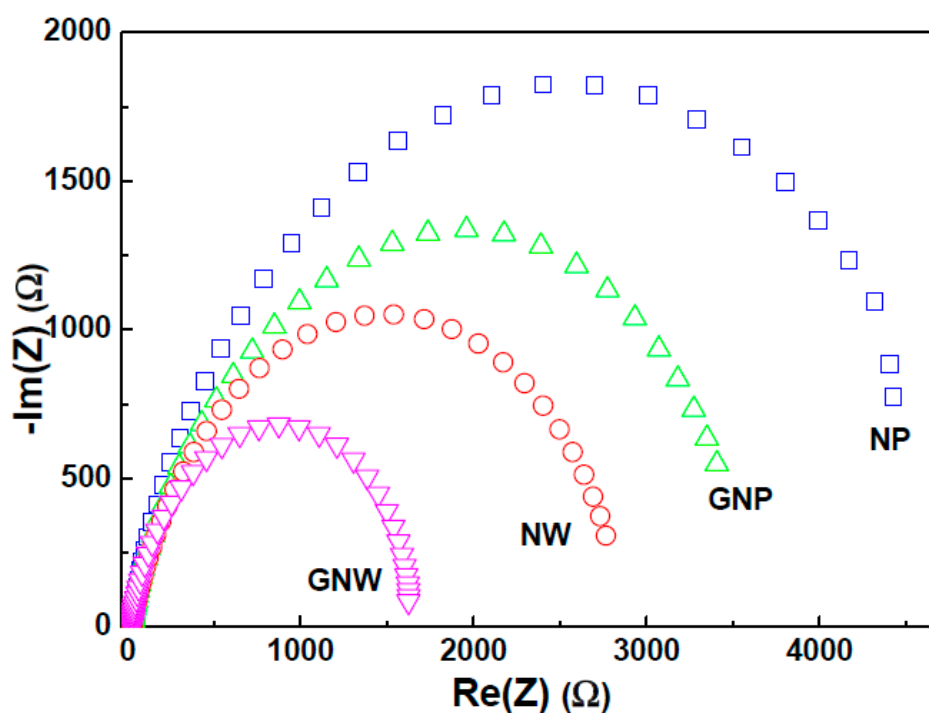


Figure 19. EIS plots of TiO₂ nanoparticles (NP), TiO₂ nanoparticles/G (GNP), TiO₂ nanowires (NW), and TiO₂ nanowires/G (GNW). Reprinted from reference [92].

Hydrothermally prepared TiO₂/G nanocomposites showed better interfacial charge transfer on the surface of G, compared to CNT or C₆₀ modified TiO₂ nanocomposites. The decrease in the radius of the semicircle in the EIS spectrum of TiO₂/G nanocomposites, compared to the spectra of the other carbon nanocomposites confirmed this improvement. Accordingly, G modified nanocomposites exhibited the highest photogenerated electrons-positive holes lifetime and photocatalytic activity, among the other carbon modified TiO₂ nanocomposites [164]. EIS results by Pan showed that the TiO₂ nanowires (NW) improved the charge separation and decreased the electron scattering than

TiO₂ nanoparticles (NP). In addition, the presence of G decreased the electron-hole recombination rate compared with their pure TiO₂ counterparts, as shown in Figure 19 [92]. The increase in the photocatalytic activity of TiO₂/G nanocomposites associated with the decrease in the electron-hole recombination rate can be measured by EIS as well as, photoluminescence (PL) spectroscopy [165].

3.4.3. Photoluminescence (PL) Spectroscopy

The recombination of photoinduced electrons and the positive holes after illumination with UV or visible light leads to the emission of photons that produce the characteristic PL peaks [127]. The introduction of G in the TiO₂/G nanocomposites is associated with substantial decline in the intensity of the PL spectrum of TiO₂ nanoparticles, as shown in Figure 20. This decrease in intensity is ascribed to the fact that G can transport the photogenerated electrons rapidly preventing the electron-hole pair recombination which is important in the enhancement of photocatalytic degradation [119,122,124,166]. Additionally, the increase in the G content increases the photocatalytic activity of the nanocomposites till an optimal content of G after which the photocatalytic activity decreases again [95,97].

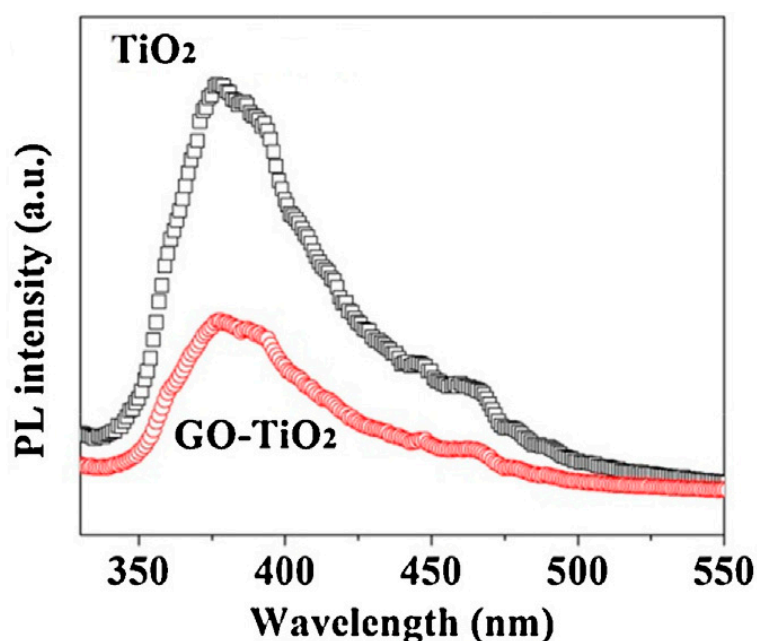


Figure 20. PL spectra of bare TiO₂ and TiO₂/GO nanocomposites. Reprinted with permission from reference [124]. Copyright 2014 Elsevier.

Graphene quantum dots (GQDs), superior electron transfer agents and excellent photosensitizers, were used to prepare TiO₂/GQDs nanocomposites with enhanced photocatalytic activity. Hao used PL to demonstrate the electron transfer improvement in the formed nanocomposites associated with the PL peak decrease. In addition, the presence of GQDs caused an apparent red shift indicating the widening in the photosensitization band of TiO₂ and the formation of Ti–O–C chemical bonds coupled with significant improvement in the photocatalytic activity, as shown in Figure 21 [167].

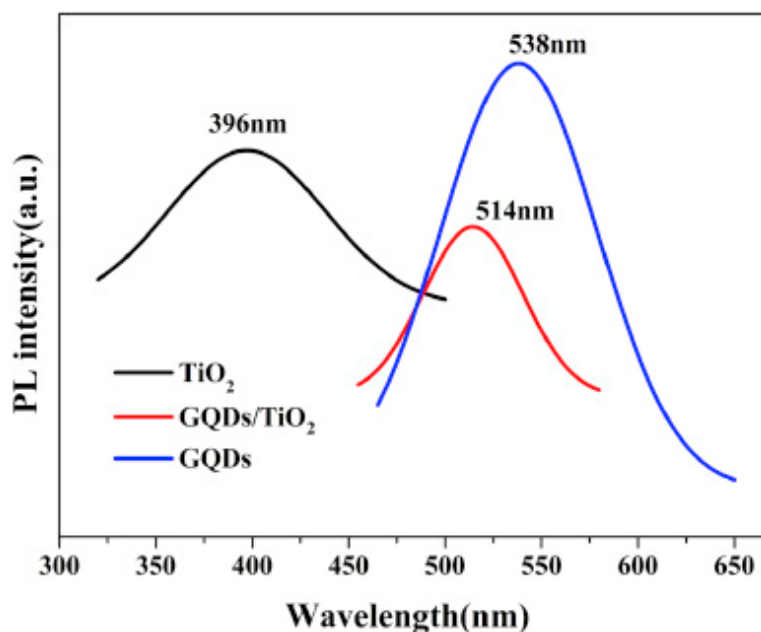


Figure 21. PL spectra of GQDs, TiO_2 , and TiO_2/GQDs . Reprinted with permission from reference [167]. Copyright 2016 Elsevier.

3.5. Compositional Analysis

3.5.1. X-ray Photoelectron Spectroscopy (XPS)

For TiO_2/G and TiO_2/GO nanocomposites, XPS spectra are used to determine the efficiency of the GO reduction to G, the chemical states of Ti, O, and C species and characteristic bonding between TiO_2 and G/GO sheets through the formation of Ti–C and Ti–O–C bonds can also be confirmed by XPS. Using XPS, Huang studied the interaction between TiO_2 and G in TiO_2/G nanocomposites, prepared by the ST method, and by mechanical mixing. The presence of an additional peak in C 1s spectrum (at 281.2 eV) of the ST prepared sample was ascribed to the formation of Ti–C bonds. This was also confirmed by the analysis of Ti 2p core level in the XPS spectra, showing the presence of the two peaks at binding energies of 458.8 and 464.6 eV attributed to ($\text{Ti } 2p_{3/2}$) and ($\text{Ti } 2p_{1/2}$) respectively for anatase [119]. Furthermore, a shift in the Ti 2p and O 1s regions to higher binding energies after the formation of the TiO_2/G nanocomposites, was related to the perturbation of the Ti–O bonds at the surface after the addition of G sheets. In addition, the increase in the G amount was associated with a shift in the binding energies of the C–C and C–O bonds [118].

XPS is used to confirm the chemical reduction of GO to G. This determination is important because the presence of residual GO in the sample may affect the TiO_2/G nanocomposites properties, hence applications. The reduction of GO to G is confirmed by observing the decrease in C 1s and O 1s peaks that correspond to oxygenated species with a concomitant increase in the C–C peak intensity as shown in Figure 22 [122]. Additionally, the decrease in the intensity of C=O peaks, which are related to carbonyl groups at the edges of the reduced GO, was attributed to their more difficult reduction [158]. In the same context, XPS was used to confirm the reduction of GO to G after ethanol and UV-induced reduction [147], ST [122], and HT treatment [93,103]. Furthermore, XPS was used to study the photocatalytic degradation products of Bisphenol A by comparing the XPS spectra of the TiO_2/G nanocomposites before and after the compound photodegradation [93]. Consequently, XPS together with FTIR/Raman spectroscopy represent the most used techniques to trace the reduction of GO to G during the formation of TiO_2/G nanocomposites.

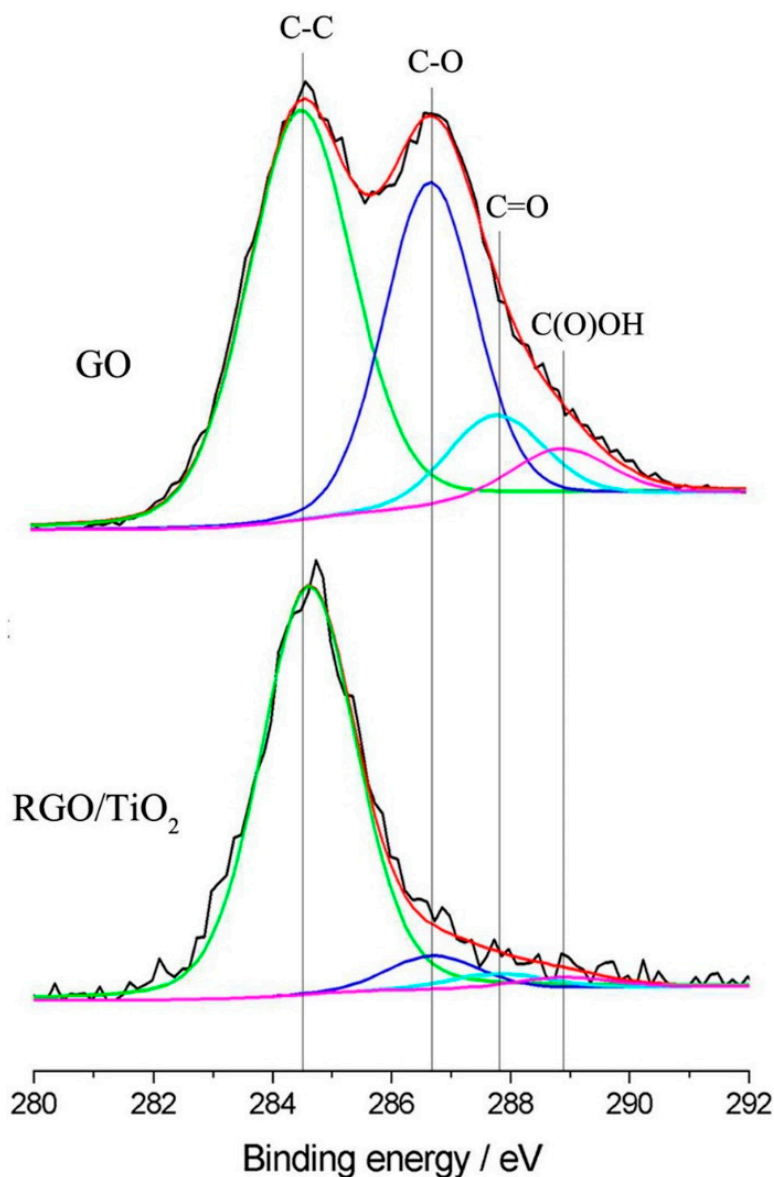


Figure 22. XPS spectra of C 1s for GO and TiO₂/RGO nanocomposites. From peak area, the reduction of GO was calculated as 76.5%. Reprinted with permission from reference [122]. Copyright 2013 American Chemical Society.

3.5.2. Raman and FTIR Spectroscopy

These two complementary techniques are discussed together. Surface Enhanced Raman spectroscopy (SERS) is a powerful technique in studying the surfaces of composite materials [151,168,169]. For example, it can provide valuable information about the number and quality of the G layers, doping level, and crystal phase structure of TiO₂ [127]. Bai used Raman spectroscopy to confirm the presence of single layer G in the TiO₂/G nanocomposites and that TiO₂ (anatase) is the most prominent crystal phase in the prepared nanocomposites as shown in Figure 23 [93]. Raman spectroscopy is also used to evaluate the efficiency of chemical reduction of GO to G by observing the frequency shifts in the Raman G bands [158]. Thermal reduction of GO to G during HT treatment can also be detected using Raman spectroscopy [98,166]. Athanasekou used a micro-Raman spectrometer to evaluate the homogeneity of the distribution of TiO₂/G nanocomposites within an ultrafiltration membrane for water treatment where decreasing the pore size of the membrane lead to an inhomogeneous distribution of the TiO₂/G nanocomposites [18].

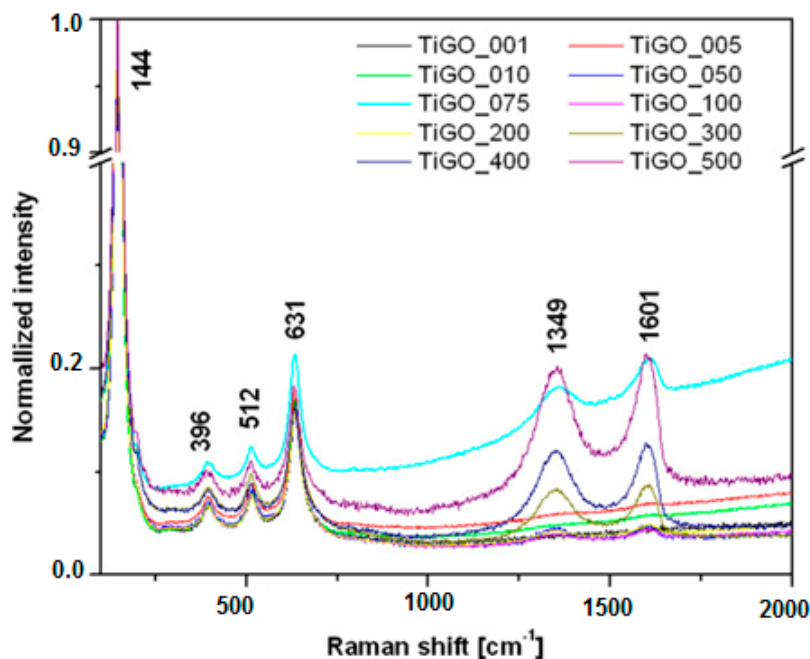


Figure 23. Raman spectra of TiO₂/GO nanocomposites with different GO amounts, adapted from reference [16].

The reduction of GO to G and the formation of Ti–C and Ti–O–C chemical bonds in TiO₂/G and TiO₂/GO nanocomposites was also confirmed by FTIR. Efficient reduction of GO is verified by the decrease and/or disappearance of the bands of oxygenated functional groups at 3000–3500, 1720, 1350 and 1050 cm⁻¹ attributed to the transformation of GO to G, as shown in Figure 24. FTIR is typically used to confirm the reduction of GO to G [97,100,127,158,170]. Diffuse reflectance FTIR (DRIFT) has been employed for the same purpose [123].

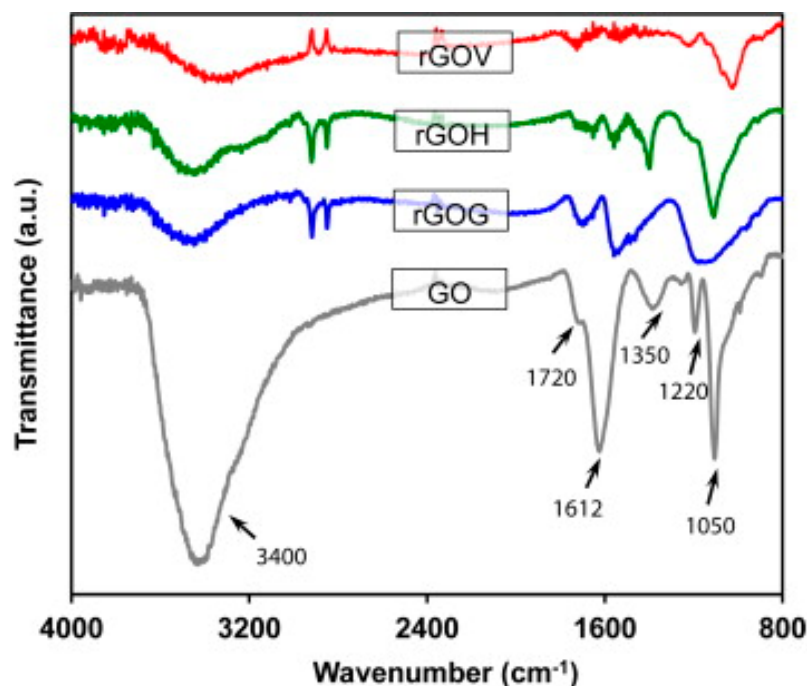


Figure 24. FT-IR spectra for GO and G prepared by reduction of GO using glucose (GOG), hydrazine (GOH) and ascorbic acid (GOV). Reprinted with permission from reference [158]. Copyright 2014 Elsevier.

3.5.3. Thermal Gravimetric Analysis (TGA)

TGA is used to analyze the amount of loaded G in TiO₂/G and GO in TiO₂/GO nanocomposites by subtracting the weight loss on heating bare TiO₂, usually in air flow conditions, from the weight loss obtained on heating the nanocomposites under the same conditions [122,141]. TGA curves of the TiO₂/G and TiO₂/GO nanocomposites involve three steps of weight loss. The first occurs below 100 °C and corresponds to the desorption of water molecules. The second step, at 200–300 °C, is due to the loss of functional groups with the release of CO_x species. Finally, the destruction of the G carbon skeleton occurs above 450 °C [94]. Figure 25 shows the three main steps of weight loss of TiO₂/G nanocomposites under TGA conditions. In addition, the second step is used to evaluate the efficiency of reduction of GO to G, where more efficient reduction of GO to G leads to the presence of less oxygenated functional groups and consequently a weaker peak in the TGA plot. This is also confirmed by using the results of TGA and differential thermal analysis (DTA) [134]. Furthermore, the thermal stability of TiO₂/G and TiO₂/GO nanocomposites can be assessed by TGA and the results show that GO exhibits more weight loss, and is, therefore, less thermally stable than G at temperatures above 300 °C due to the loss of the oxygenated functionalities [158]. The same technique showed that the chemically bonded TiO₂/G nanocomposites prepared by the ST method had the onset of weight loss occurring at higher temperatures than that of mechanically mixed TiO₂/G nanocomposites, suggesting the formation of more thermally stable Ti–C chemical bonds [119,123].

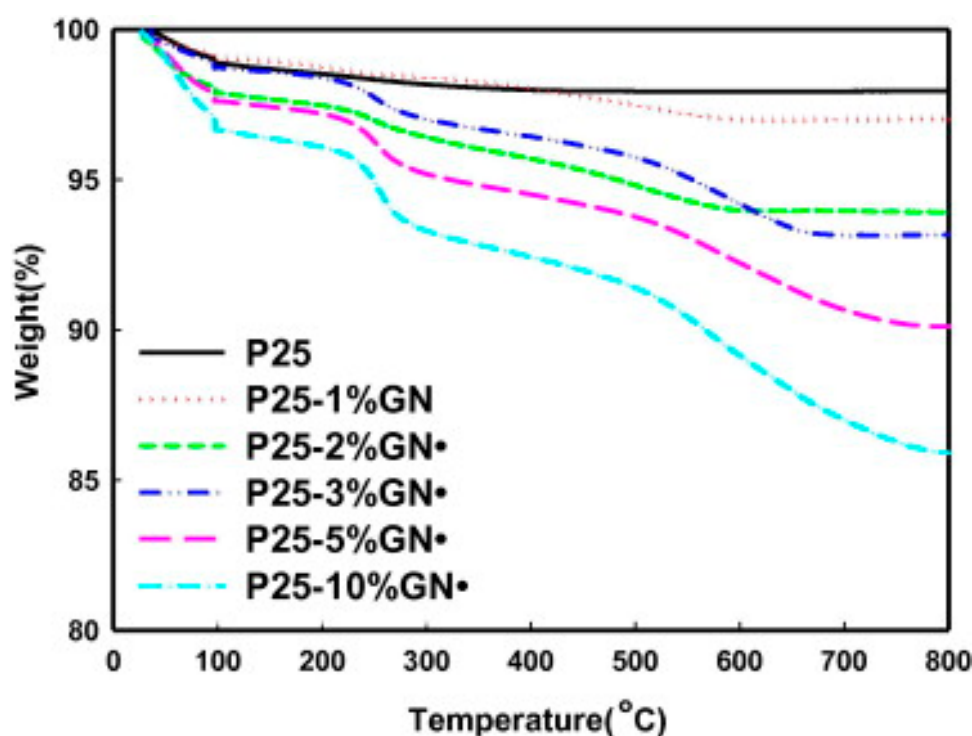


Figure 25. TGA curves for TiO₂ (P25) and TiO₂/G nanocomposites with different amounts of G. Reprinted with permission from reference [94]. Copyright 2013 Elsevier.

3.5.4. Electron Spin Resonance (ESR)

As discussed above, the mechanism of the photocatalytic degradation by TiO₂/G and TiO₂/GO nanocomposites depends mainly on the formation of intermediate radicals such as •OH and O₂•⁻/HO₂•. The presence of these radicals can be evaluated using ESR. However, due to their short lifetimes and high reactivity, 5,5-Dimethyl-1-pyrroline-N-oxide (DMPO) is commonly used to trap these radicals forming a relatively stable species, as reflected in Figure 26. Experimental investigations demonstrated the presence of more intense signal for •OH under UV light irradiation during the photocatalytic process as compared with signals for O₂•⁻/HO₂•. These results were

attributed to the conversion of the superoxide species $O_2^{\bullet-}/HO_2^{\bullet}$ to hydroxyl radicals $\bullet OH$ under UV light illumination increasing the intensity of the latter with a consequent increase in the photocatalytic activity [122,171].

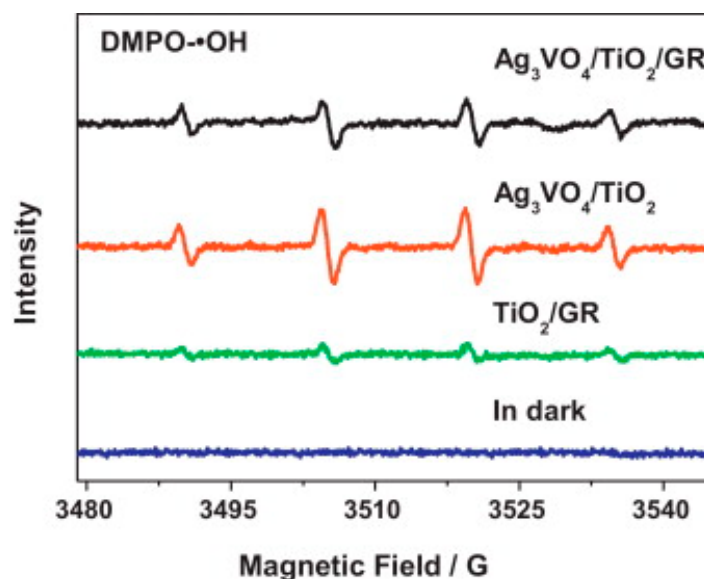


Figure 26. ESR spectra showing the formation of stable DMPO-based free radicals formed when doped TiO_2 -GR is irradiated with visible light. Reprinted with permission from reference [171]. Copyright 2013 Elsevier.

3.6. Microscopic Surface Properties

Determining the surface properties on the microscopic level of a catalytic material is relevant to its application because these surface properties have a significant impact on the adsorption/desorption processes on the catalyst surface, and on the physico-chemical processes taking place therein. In this respect, surface properties, such as the number, location, and strength of acidic and basic sites on the catalytic surface, as well as surface polarity and surface polarizability play a key role in the catalytic activity of the catalyst and hence its applications [172–174]. Surface free energy, determined by inverse gas chromatography, is used to determine the acidic and basic properties of solid surfaces accurately over a wide range of temperature [175,176]. This technique was used successfully to investigate the surface properties of G and GO [177]. However, very few techniques are used to systemically study these microscopic surface properties and their effect on the photocatalytic applications of TiO_2/G and TiO_2/GO nanocomposites; these are described below.

3.6.1. Point of Zero Charge (pH_{PZC}) Measurements

The point of zero charge (pH_{PZC}) is measured using a pH drift test where unbuffered solutions with variable pH values (2 to 12) are put into contact with the TiO_2/G and TiO_2/GO nanocomposites for some time, e.g., 24 h, and the final pH is recorded [158]. The pH_{PZC} of TiO_2/GO nanocomposites decreases with the increase in the GO content. The decrease in the pH_{PZC} indicates the increase in surface Brønsted acidity of the nanocomposites which is ascribed to the oxygenated functional groups on the surface of the GO. On the other hand, thermal treatment of the TiO_2/GO nanocomposites causes partial reduction of the surface acidic groups, which is confirmed by the increase in the value of pH_{PZC} with increasing treatment temperature [123]. Furthermore, pH_{PZC} is used to explain the higher photodegradation rate of methylene blue (MB) dye using TiO_2/GO nanocomposites relative to the photocatalytic degradation of methyl orange (MO) dye. The negative charge on the surface of the TiO_2/GO nanocomposites at pH values of 6 to 7.2, due to the dissociated surface groups, leads to efficient binding of cationic MB. This increases the photocatalytic efficiency. On the other hand,

the low pK_a value of MO indicates weak adsorption of the negatively-charged species on TiO_2/GO nanocomposites [18].

3.6.2. Temperature Programmed Desorption (TPD)

TPD is used to calculate the amounts of different oxygenated surface functional groups that evolve as CO and CO_2 after heating the TiO_2/G and TiO_2/GO nanocomposites under an inert atmosphere, e.g., helium. The lower evolution of CO and CO_2 under TPD conditions for the G containing nanocomposites, compared to GO, is due to the lower number of oxygenated functionalities on the G surface. These findings are used as an effective method to evaluate the reduction efficiency of the GO using different reducing agents. For example, the amount of CO_2 released by TPD of GO was $5305 \mu\text{mol/g}$, and the amounts released by TPD of GO reduced by hydrazine, ascorbic acid, and glucose, were 957, 1215, and $1056 \mu\text{mol/g}$, respectively [158]. Furthermore, the deconvolution of the CO and CO_2 profiles is used to study the surface oxygenated functional groups in details. The CO_2 -TPD profile deconvolution revealed that the surface of GO is covered with hydroxyl, epoxy, carboxylic acid, carboxylic anhydride, and lactone functional groups. On the other hand, the CO-TPD profiles of GO-containing composites include peaks that correspond to the presence of phenols, ethers, carbonyls, and quinones. Furthermore, the analysis of the TPD spectra for the G-containing composites shows that the reduction process affects mainly the hydroxyl and epoxy groups, as demonstrated in Figure 27 [158].

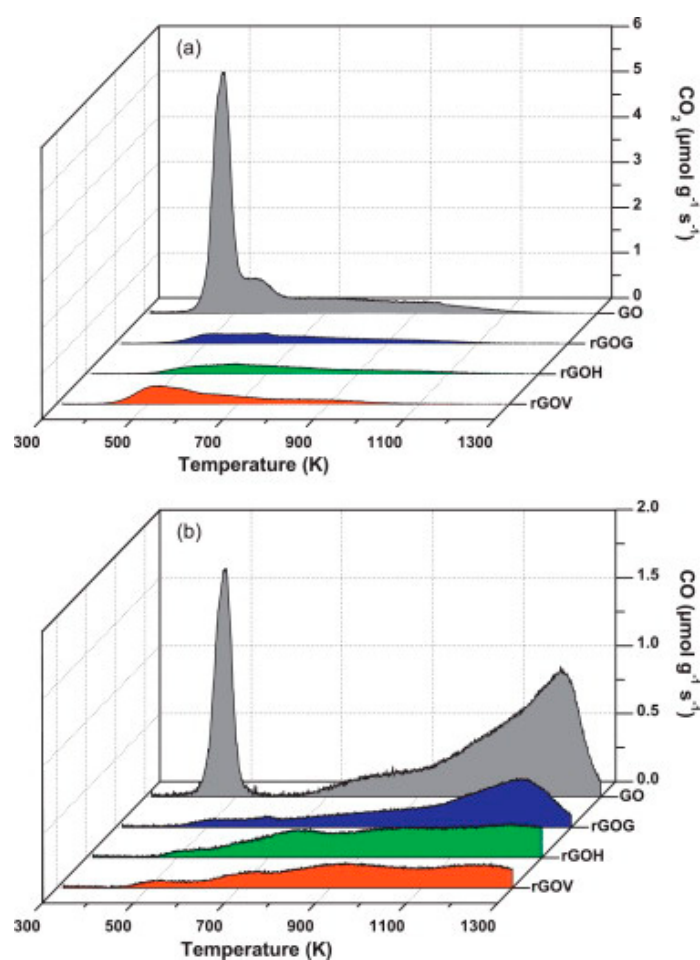


Figure 27. TPD profiles for the release of CO_2 (a) and CO (b) from GO and reduced GO using glucose (GOG), hydrazine (GOH) and ascorbic acid (GOV). Reprinted with permission from reference [158]. Copyright 2014 Elsevier.

TPD is also commonly used to determine the number of the surface acidic and basic sites using the adsorption/desorption of NH_3 and CO_2 respectively. The use of NH_3 -TPD method determines the overall surface acidity of solid materials, without distinction between Lewis acidity and Brønsted acidity [178]. Recently, NH_3 -TPD was used to measure the overall surface acidity of TiO_2/G and TiO_2/GO nanocomposites. The overall surface acidity of TiO_2/GO nanocomposites was higher than the overall surface acidity of bare TiO_2 and TiO_2/G nanocomposites. This was ascribed to the presence of oxygenated functional groups on the surface of GO sheets [178].

4. TiO_2/G and TiO_2/GO Photocatalytic Applications for the Decomposition of Water Contaminants

Removal of environmental pollutants using photocatalysis is very promising for water treatment, filtration, self-cleaning and other various applications. As discussed above, the enhancement of TiO_2/G and TiO_2/GO nanocomposites as photocatalysts, relative to bare TiO_2 is attributed to a combination of: (i) inhibition of photoinduced electrons-hole pair recombination caused by G acting as electron sink for these photoinduced electrons; (ii) increase in the lifetime of the photogenerated electrons-hole pairs; (iii) narrowing of the band gap and red shift in light absorption that improves the photocatalytic activity of the formed nanocomposites; (iv) increase in the adsorption of the dye molecules on the surface of the nanocomposite relative due to enhanced surface area and the strong π - π interaction between the dye and the aromatic network of G [95].

Some applications of TiO_2/G and TiO_2/GO nanocomposites for the removal of environmental water pollutants are briefly presented below.

4.1. Photocatalytic Degradation of Dyes

MB dye is typically used as a model pollutant to study photocatalytic activity. This is due to the presence of large amounts of MB in industrial wastewater from paints, dye production and textiles manufacturers plus the difficulty in the removal of MB by usual degradation methods [95,179]. MB is considered by the international organization for standardization (ISO) as the standard test for photocatalytic film activity [180]. The photocatalytic degradation of MB under UV-Vis light irradiation is usually described by pseudo-first order kinetics [95,160].

Shi prepared N-doped TiO_2/G nanocomposites (NTS/G), where TiO_2 were in the form of anatase plates with exposed {001} facets using one-pot HT method. The prepared NTS/G nanocomposites exhibited higher degradation rate for MB in comparison to the NTS without G. This enhanced photodegradation (measured at $\lambda > 420$ nm) confirmed that the presence of G in the nanocomposites is responsible for this improvement. The nanocomposite samples prepared by adding 6 mL of GO aqueous solution during the HT preparation, showed a better photodegradation of MB than the samples prepared by adding 2, 4, 8 and 10 mL of GO aqueous solution, respectively. This implied that increasing the amount of G had a competing effect between enhancing the photocatalytic degradation rate of MB and decreasing the light absorption of the photocatalyst itself, as shown in Figure 28. An optimal amount of G in the nanocomposites gives a maximum photocatalytic activity for the degradation of MB dye [95].

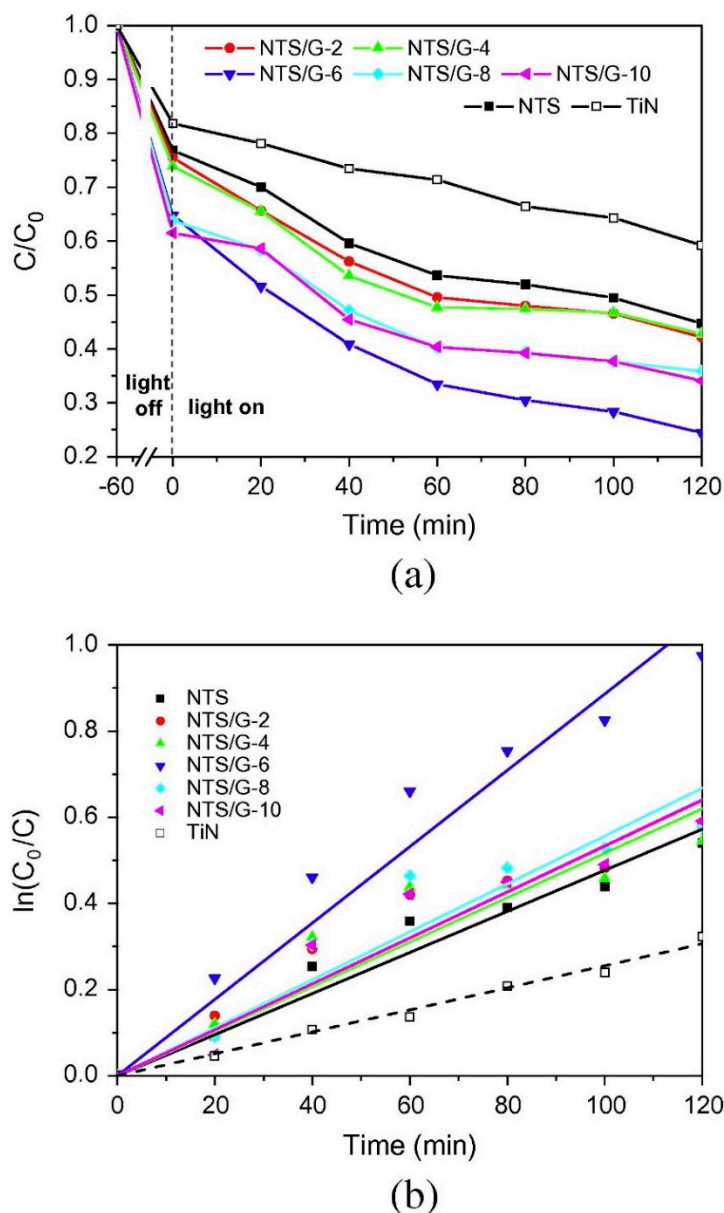


Figure 28. (a) Photodegradation of MB over TiO_2/G nanocomposites with different amounts of G under visible light illumination, and (b) pseudo-first order reaction kinetics of MB photodecomposition. Reprinted with permission from reference [95]. Copyright 2014 Elsevier.

Recyclable magnetic TiO_2/G nanocomposites are produced using GO loaded with TiO_2 nanoparticles and SiO_2 insulated magnetite aggregates followed by HT treatment to reduce GO to G. The prepared nanocomposites enhanced the photodegradation rate of MB by 20%, relative to commercial TiO_2 (P25). Although the enhancement is modest, catalyst recovery is simply achieved by exposing the used nanocomposites to a magnetic field for ca. 1 min, to collect the nanocomposites, followed by UV treatment for an extended time to remove any remaining organic contaminants [98].

The addition of CNTs to the TiO_2/G nanocomposites improves the photodegradation of MB by a 2.2-fold. This was ascribed to the decrease in the recombination of photoinduced electron-hole pairs caused by both G and CNTs which is confirmed by the increase in the number of formed hydroxyl radicals in presence of CNTs [116].

The addition of G can improve the photodegradation of MB by a photothermal effect (PTE) which contributed ~38% to dye degradation. This new mechanism of photocatalytic enhancement caused by G was proposed by Gan. TiO_2/G nanocomposites were prepared by an HT method with different

amounts of G. The 5 wt% sample showed the highest photocatalytic effect. The PTE was induced using near-infrared (NIR) radiation, representing a significant part of sunlight radiation. This work implies that the role of PTE of solar radiation in the photodegradation process is enhanced by the addition of G [181]. TiO₂/G nanocomposites prepared using microwave-assisted synthesis with deposited TiO₂ nanoparticles on the G sheets, have improved visible light absorption. This was ascribed to the formation of Ti–O–C bonds as compared to the nanocomposites prepared by mechanical mixing. The higher photocatalytic performance under xenon lamp irradiation of the former compared to the latter is confirmed using the photodegradation of MB. The microwave-assisted sample decomposed MB from an original concentration of 10 mg/L to ca. 0.5 mg/L in 5 h. The mechanically mixed sample, on the other hand, resulted in a final concentration of ca. 4 mg/L [148].

TiO₂/G nanocomposites containing strongly wrapped G onto TiO₂ nanoparticles were prepared by Ni. They mixed amine-functionalized TiO₂ nanoparticles with different amounts of GO aqueous dispersions under vigorous stirring, followed by HT treatment to reduce GO to G. Compared to the nanocomposites prepared without amine functionalization, the amine-functionalized TiO₂/G nanocomposites exhibited higher photodegradation of MB of about 7-fold increase in MB degradation after 120 min. The higher photocatalytic activity was a result of the strong interaction between G and TiO₂ after wrapping. This interaction decreased the band gap in these samples. The researchers also reported that increasing the amount of added G increased the photocatalytic activity till a content of 2 wt% G, followed by a subsequent reduction in the photocatalytic activity with further increase of G due to the interference with the light absorption [97]. Zhang prepared multifunctional TiO₂/G hydrogels using a one-pot HT method. The formed TiO₂/G hydrogels had better photocatalytic degradation of MB compared to pristine TiO₂ nanoparticles [103]. The effect of the presence of different oxidants on the photodegradation of MB by TiO₂/G nanocomposites was investigated by Sun. They reported better photodegradation of MB under visible light compared to UV irradiation. In addition, the effect of hydrogen peroxide (H₂O₂) as an oxidizing agent on the photodegradation of MB was superior to other oxidants such as peroxymonosulfate and peroxydisulfate. The improved effect of H₂O₂ was attributed to a lower quenching effect and higher trapping of the photoinduced electrons [160]. Photodegradation of both cationic MB, and anionic Congo red, dyes was achieved using biphasic TiO₂/G nanocomposites prepared by HT method. Compared to UV-filtered light, natural sunlight improved the photodegradation of both dyes which implies the importance of the UV part of natural sunlight [182].

The photodegradation of reactive black-5 dye (RBK-5) was evaluated using TiO₂/G nanocomposites prepared from P25 TiO₂ with different amounts of G ranging from 1 to 10 wt% in an HT process. The degradation removal efficiency for RBK-5 for the TiO₂/G nanocomposites was improved compared to the P25, reaching more than 90% under UV radiation. However, the change in G content showed no significant variation in the degradation removal efficiency [94]. On the other hand, acid orange 7 (AO7), a common dye used in textile industry, was fully degraded using TiO₂/G nanocomposite under UV light irradiation within 20 min. This improved photodegradation was ascribed to the formation of the strongly oxidizing (\bullet OH), as a result of the favorable effect of G on the separation between the photoinduced electrons and positive holes [124]. In addition, the improved AO7 photodegradation using N-doped, N and V co-doped TiO₂/G and TiO₂/GO nanocomposites under visible light irradiation was attributed to the enhancement of dye adsorption and light absorption, extended photogenerated pairs lifetime, and photosensitizing effect of G on the doped nanocomposites [90].

TiO₂/G nanocomposites showed improved photodegradation of rhodamine B dye under visible light irradiation due to the strong chemical interaction between the OH groups on the surface of TiO₂/G nanocomposites and the COOH group of the dye molecule. The presence of P123 nonionic surfactant, a triblock copolymer, during the nanocomposite formation decreased TiO₂ nanoparticles aggregation and increased the surface area and this combined effect further improved the photodegradation of rhodamine B and increased the catalytic stability of the formed nanocomposites [118]. The presence of

GO in TiO₂/GO nanocomposites prepared by two-step HT synthesis, improved the photodegradation of rhodamine B by a three-fold increase over P25. During the HT synthesis ethanol/water mixed solvent and sulfuric acid were used to enhance the growth of TiO₂ on the GO sheets and decrease the growth of free TiO₂ nanoparticles in the solution [183].

4.2. Photocatalytic Degradation of Chemicals and Pharmaceuticals

Groundwater contaminated by domestic wastewater is likely to contain small amounts of chemicals that are clearly of anthropogenic origin, e.g., caffeine and pharmaceuticals, calling for new methods of decontamination. The use of TiO₂/G and TiO₂/GO nanocomposites as photocatalysts for the degradation of pharmaceuticals has increased in the recent years. Recyclable magnetic TiO₂/G nanocomposites exhibited improved photodegradation of caffeine and carbamazepine, an anti-epileptic drug [98]. Carbamazepine was efficiently removed from water using TiO₂/G nanocomposites prepared by the microwave-hydrothermal method under UV-A light irradiation [184] and by TiO₂/G aerogels prepared by HT method [185]. Photodegradation of three aromatic pharmaceuticals, carbamazepine, sulfamethoxazole antibacterial and ibuprofen anti-inflammatory, using TiO₂/G and TiO₂/Fe nanocomposites under both visible and UV light irradiation. TiO₂/G nanocomposites showed higher photocatalytic activity under UV light irradiation ascribed to the decreased rate of recombination between electron-hole pairs. On the other hand, TiO₂/Fe nanocomposites exhibited higher photodegradation under visible light irradiation attributed to efficient band gap narrowing [51]. Moreover, the immobilization of TiO₂/G nanocomposites on optical fibers improved the photocatalytic degradation of these three aromatic pharmaceuticals in aqueous solutions [186].

Diphenhydramine (DP) is one of the most widely used anti-histaminic drugs and the third most detected healthcare product in the liver of fish collected from different locations in the United States. The low biodegradation and high toxicity of DP prompted Pastrana-Martínez to study the photodegradation of DP using TiO₂/G and TiO₂/GO nanocomposites. The results showed that TiO₂/GO nanocomposites had a higher DP photodegradation rate compared to TiO₂/G nanocomposites under both UV-Vis and visible light irradiation. The improved photoactivity was attributed to the more efficient distribution of TiO₂ on GO sheets [158]. Moreover, the photodegradation of DP using TiO₂/G nanocomposites is achieved using direct oxidation by the photoinduced holes rather than reduction by the photogenerated electrons as reported in another work by the same group [138]. In this context, the effect of different treatment temperatures on the photodegradation of DP using TiO₂/G nanocomposites was also studied [123].

TiO₂/GO nanocomposites prepared by LPD, achieved improved photocatalytic degradation of four priority pesticide residues: alachlor, atrazine, diuron and isoproturon in both ultrapure and natural water samples [187]. Li investigated the effect of different G contents in TiO₂/G nanocomposites on the photodegradation of aldicarb pesticide, and norfloxacin antibiotic. G content of 0.86 wt% exhibited the best photocatalytic performance [118]. The thickness of the TiO₂ layer in TiO₂/Fe₃O₄/G nanocomposites affected the photodegradation rate of enrofloxacin antibiotic and the optimum thickness was 17 nm ascribed to a maximum balance between effective photogeneration and transport of electrons [188]. The effect of the synthesis method was studied by Gholamvande for the photodegradation of famotidine, an anti-ulcer drug, as a model water pollutant. TiO₂/G nanocomposites, prepared by sol-gel method exhibited 90% decrease in the initial famotidine concentration after 45 min compared to 50% and 30% decrease for the TiO₂/G mechanically mixed and pure TiO₂ powder, respectively [189]. Antipsychotic, risperidone, was successfully removed from different water samples, including distilled, tap, river and lake water. TiO₂/G nanocomposites enhanced the photodegradation of risperidone, compared to TiO₂ nanoparticles, in all tested samples and the effect was directly proportional to the G amount till 20%, as reported by Calza [190]. Chlortetracycline, a persistent antibiotic in aquatic environments, was successfully removed using TiO₂/GO nanocomposites prepared by mixing TBT and GO dispersions in ethanol/water

mixture. The effect of pH was studied and weakly acidic conditions, pH 4, exhibited the highest photodegradation rate [191].

The herbicide 2,4-dichlorophenoxy acetic acid is used worldwide in agriculture and is present in large amounts in wastewater. It was efficiently removed using TiO₂/G nanocomposites doped with noble metals as Platinum (Pt) under UV-Vis light due to the large surface area and the decrease in the electron-hole recombination in addition to the high photonic efficiency caused by the noble metal [17]. Acetic acid photooxidation using TiO₂/G nanocomposites under visible light irradiation was studied by Morawski [192]. The photodegradation of bisphenol A, an environmental pollutant, was evaluated using TiO₂/G nanocomposites with uniform TiO₂ nanoparticles distribution and enhanced photocatalytic activity under UV and visible light irradiation. The degradation resulted in all carbon atoms of bisphenol A converting to CO₂ [93]. Hydrothermally prepared TiO₂/GO nanocomposites were used by Fu to study the photocatalytic degradation of phenol. Cost analysis of the prepared nanocomposites showed the economic feasibility of using TiO₂/GO nanocomposites in removing phenolic compounds from water. The photodegradation rate constant is almost doubled for the formed nanocomposites compared to other photocatalysts, as Cu-TiO₂ [193].

Naphthenic acids, produced by extraction of bitumen, represents a challenge in wastewater treatment due to the complex chemical structure. TiO₂/G nanocomposites prepared by ST method represent a promising solution, due to the efficient charge separation and increased surface area, naphthenic acid photodegradation showed promising results at pH 3. The study of the reactive species, involved in the photodegradation process, revealed that positive holes and HO• are the most prominent, as confirmed using ethylenediaminetetraacetic (EDTA) acid disodium salt as hole scavenger and isopropanol as radical scavenger [194].

4.3. Other Applications for Water Decontamination

Combining photocatalysis and filtration processes are beneficial to synergistically improve water decontamination from different pollutants. A hybrid photocatalytic/ultrafiltration system was produced using TiO₂/G nanocomposites deposited into the pores of monolith filters using a dip-coating technique. The prepared membranes were tested for the elimination of MB and MO dyes under UV and visible light irradiation. The effect of the pore size of the monoliths filters was studied and the elimination of both dyes using the novel hybrid membrane was better than the standard nanofiltration process [18]. In addition, the antifouling effect of TiO₂/GO hierarchical filtration membrane under UV irradiation was demonstrated by the effective removal of organic dyes (Direct Red 80 and Direct Blue 15) [141]. A Polypropylene filter modified with TiO₂/G, exhibited a higher rate of elimination of MB under halogen lamp irradiation as compared with the TiO₂-modified filter [99].

Gao used the layer by layer methodology to deposit TiO₂/GO nanocomposites on the surface of polysulfone base membrane. The prepared membrane increased the elimination of MB, as a model contaminant, under both UV and sunlight irradiation with higher efficiency under sunlight irradiation of ca. four-fold more than the TiO₂ modified membrane, without G. The prepared membrane showed also a three-fold increase in the membrane flux under UV light, this was ascribed to the membrane hydrophilicity due to TiO₂ and GO and the photoinduced contaminant degradation [147]. Another variation involved the use of the dip-coating technique to prepare hydrophilic polyacrylic acid coating with antibacterial and self-cleaning properties using TiO₂/G nanocomposites. High photocatalytic activity, stability, and hydrophilicity render this coating as a potential enhancement in antibacterial coatings [195].

Other environmental photocatalytic applications of TiO₂/G and TiO₂/GO nanocomposites include the photocatalytic removal of fulvic acid, a natural organic matter that increases the level of heavy metals and adsorbed organic pollutants in drinking water. The improved adsorption and photodegradation of fulvic acid by TiO₂/G nanocomposites under UV light irradiation were attributed to the presence of G sheets in the formed nanocomposites [196]. The photoreduction of Cr(VI) to Cr(III) under UV light irradiation using TiO₂/G/CNTs composites was evaluated. The results showed that

the photoreduction of Cr(VI) was dependent on the released electrons from the valence band of TiO₂ to G, where CNTs enhances this transfer by acting as a charge transmitting path, rather than the formation of positive holes that affect the oxidation of dyes as MB [116]. Liu reported the increase in surface area enhanced the photoreduction of Cr(VI) under visible light irradiation [56]. Photocatalytic removal of radioactive uranium (VI) from aqueous solutions was achieved using TiO₂/Fe₃O₄/G nanocomposites. The presence of G improved the photocatalytic efficiency as well as decreased the photo dissolution of Fe₃O₄ compared to TiO₂/Fe₃O₄ composites. The prepared nanoparticles were easily recovered by exposure to magnetic fields, thus the recyclability of the nanocomposites was achieved [197].

Photodecomposition of the bromate, a carcinogenic contaminant found in drinking water, into bromide ion using TiO₂/G nanocomposites under UV light illumination was studied by Huang. The best photocatalytic performance was found for 1%wt content G at pH 6.8. The decrease in bromate concentration with concomitant increase in bromide level, at nearly the same amount of total bromine content, proved that the photodecomposition of bromate is primarily due to photoreduction rather than adsorption [166]. The disinfection of *Escherichia coli* (*E. coli*) using TiO₂/GO nanocomposites in solar light was attributed to the strong oxidant activity of hydroxyl radicals (\bullet OH) generated from the interaction of dissolved oxygen and water molecules with the positive holes on the surface of the nanocomposites [124].

5. Conclusions

Nanocomposites of TiO₂ with G and GO are obtained, inter alia, by thermal methods, sol-gel process, mechanical mixing with or without sonication, and deposition either in the liquid phase, gas phase, or as a film. Compared to bare TiO₂, the produced nanocomposites have smaller bandgap energies, slower rates of recombination between the photoinduced electrons and the holes on the TiO₂ surface, and larger surface areas. The latter, leading to enhanced contaminant adsorption, represents a primary advantage of TiO₂ nanocomposites with G and GO relative to doped TiO₂ which could possibly exhibit higher photocatalytic activity. These changes in the physicochemical properties of TiO₂/G and TiO₂/GO are determined by an array of techniques, based on diffraction (X-ray), spectroscopy (UV-Vis, FTIR, Raman, EPR), microscopy (SEM and TEM), adsorption/desorption of gases (BET) etc.

The decrease in the band gap energy leads to absorbance in the visible region of the spectrum, i.e., it turns photo-oxidation by sunlight feasible, in contrast to using UV radiation with bare TiO₂. The catalytic efficiency is further enhanced by the concomitant increase in the lifetime of the charge carriers, and catalyst surface area. This leads to higher adsorption of aromatic pollutants, e.g., azo dyes, due to their strong π - π interactions with the aromatic network of G and GO. We hope that this review contributes to increasing the interest in the development of efficient photocatalysts, and their application to solving some pressing global problems, especially water pollution.

Supplementary Materials: The following are available online at <http://www.mdpi.com/2073-4344/8/11/491/s1>, Table S1: Synthesis, characterization, and applications of TiO₂/G and TiO₂/GO nanocomposites in the literature.

Funding: This research received no external funding.

Acknowledgments: O.A.E. thanks FAPESP (São Paulo State Research Foundation) for financial support of a part of this work, and CNPq (National Council for Scientific and Technological Development, Brazil) for a research productivity fellowship. A.R.R. and A.T. thank The American University in Cairo for a graduate student research grant.

Conflicts of Interest: The authors declare no conflict of interest.

Abbreviations

AD	Aerosol deposition
AFM	atomic force microscopy
AO7	acid orange 7
BET	Brunauer–Emmett–Teller
BPA	bisphenol A
CB	conduction band
CNTs	carbon nanotubes
CVD	chemical vapor deposition
DFT	density functional theory
DMPO	5,5-Dimethyl-1-pyrroline-N-oxide
DMSO	dimethylsulfoxide
DP	diphenhydramine
DRIFT	diffuse reflectance Fourier transform infrared spectroscopy
DRS-UV	diffuse reflectance UV–Vis spectroscopy
DTA	differential thermal analysis
<i>E. coli</i>	<i>Escherichia coli</i>
EDTA	ethylenediaminetetraacetic acid
EDX	energy dispersive X-ray analysis
EIS	electrochemical impedance spectroscopy
ESR	electron spin resonance
FTIR	Fourier transform infrared spectroscopy
G	graphene
GO	graphene oxide
GQDs	graphene quantum dots
H ₂ O ₂	Hydrogen peroxide
HT	hydrothermal
ISO	international organization of standardization
LBL	layer by layer
LPD	liquid phase deposition
MB	methylene blue
MO	methyl orange
MWCNTs	multi-wall carbon nanotubes
N,V–TiO ₂ –G	Nitrogen and Vanadium co-doped TiO ₂ /G nanocomposites
NIR	near-infrared
NTS/G	Nitrogen-doped TiO ₂ /graphene nanocomposites
P123	triblock copolymer of poly(ethylene glycol)-poly(propylene glycol)-poly(ethylene glycol)
pHPZC	the point zero of charge
PL	photoluminescence spectroscopy
PMMA	poly(methyl methacrylate)
PTE	photothermal effect
PTFE	polytetrafluoroethylene
PVAc	polyvinyl acetate
RBK-5	reactive black-5
SEM	scanning electron microscopy
SERS	surface enhanced Raman spectroscopy
ST	solvothermal
TBT	tetrabutyl-titanate
TEA	triethanolamine
TEM	transmission electron microscopy
TGA	thermal gravimetric analysis

TiN	Titanium nitride
TiO ₂ /GO NRCs	TiO ₂ /GO nanorods composites
TiOSO ₄	Titanium oxysulfate
TPD	temperature programmed desorption
VB	valence band
XPS	X-ray photoelectron spectroscopy
XRD	X-ray diffraction

References

1. Schneider, J.; Matsuoka, M.; Takeuchi, M.; Zhang, J.; Horiuchi, Y.; Anpo, M.; Bahnemann, D.W. Understanding TiO₂ Photocatalysis: Mechanisms and Materials. *Chem. Rev.* **2014**, *114*, 9919–9968. [[CrossRef](#)] [[PubMed](#)]
2. Smalley, R.E. Top Ten Problems of Humanity for Next 50 Years. In *Energy & Nano Technology Conference*; Rice University: Houston, TX, USA, 2003.
3. Kant, R. Textile dyeing industry an environmental hazard. *Nat. Sci.* **2012**, *4*, 22–26. [[CrossRef](#)]
4. Zollinger, H. Colour Chemistry-Synthesis, Properties of Organic Dyes and Pigments. In *Colour Chemistry-Synthesis, Properties of Organic Dyes and Pigments*; VCH: New York, NY, USA, 1987; pp. 92–100.
5. Gupta, V.K.; Suhas. Application of low-cost adsorbents for dye removal—A review. *J. Environ. Manag.* **2009**, *90*, 2313–2342. [[CrossRef](#)] [[PubMed](#)]
6. Slokar, Y.M.; Majcen Le Marechal, A. Methods of decoloration of textile wastewaters. *Dyes Pigments* **1998**, *37*, 335–356. [[CrossRef](#)]
7. Pagga, U.; Brown, D. The degradation of dyestuffs: Part II Behaviour of dyestuffs in aerobic biodegradation tests. *Chemosphere* **1986**, *15*, 479–491. [[CrossRef](#)]
8. Willmott, N.; Guthrie, J.; Nelson, G. The biotechnology approach to colour removal from textile effluent. *J. Soc. Dyers Colour.* **1998**, *114*, 38–41. [[CrossRef](#)]
9. Pearce, C.I.; Lloyd, J.R.; Guthrie, J.T. The removal of colour from textile wastewater using whole bacterial cells: A review. *Dyes Pigments* **2003**, *58*, 179–196. [[CrossRef](#)]
10. De Mendonça, V.R.; Mourão, H.L.; Malagutti, A.R.; Ribeiro, C. The role of the relative dye/photocatalyst concentration in TiO₂ assisted photodegradation process. *Photochem. Photobiol.* **2014**, *90*, 66–72. [[CrossRef](#)] [[PubMed](#)]
11. Tao, H.; Liang, X.; Zhang, Q.; Chang, C.T. Enhanced photoactivity of graphene/titanium dioxide nanotubes for removal of Acetaminophen. *Appl. Surf. Sci.* **2015**, *324*, 258–264. [[CrossRef](#)]
12. Raghavan, N.; Thangavel, S.; Venugopal, G. Enhanced photocatalytic degradation of methylene blue by reduced graphene-oxide/titanium dioxide/zinc oxide ternary nanocomposites. *Mater. Sci. Semicond. Process.* **2015**, *30*, 321–329. [[CrossRef](#)]
13. Forgacs, E.; Cserhádi, T.; Oros, G. Removal of synthetic dyes from wastewaters: A review. *Environ. Int.* **2004**, *30*, 953–971. [[CrossRef](#)] [[PubMed](#)]
14. Namboodri, C.G.; Walsh, W.K. Ultraviolet light/hydrogen peroxide system for decolorizing spent reactive waste water. *Am. Dyest. Report.* **1996**, *85*, 15–25. [[CrossRef](#)]
15. Robinson, T.; McMullan, G.; Marchant, R.; Nigam, P. Remediation of dyes in textile effluent: A critical review on current treatment technologies with a proposed alternative. *Bioresour. Technol.* **2001**, *77*, 247–255. [[CrossRef](#)]
16. Stengl, V.; Bakardjieva, S.; Grygar, T.M.; Bludská, J.; Kormunda, M. TiO₂-graphene oxide nanocomposite as advanced photocatalytic materials. *Chem. Cent. J.* **2013**, *7*, 41–52. [[CrossRef](#)] [[PubMed](#)]
17. Ghasemi, S.; Esfandiari, A.; Rahman Setayesh, S.; Habibi-Yangjeh, A.; Iraj Zad, A.; Gholami, M.R. Synthesis and characterization of TiO₂-graphene nanocomposites modified with noble metals as a photocatalyst for degradation of pollutants. *Appl. Catal. A Gen.* **2013**, *462–463*, 82–90. [[CrossRef](#)]
18. Athanasekou, C.P.; Morales-Torres, S.; Likodimos, V.; Romanos, G.E.; Pastrana-Martinez, L.M.; Falaras, P.; Faria, J.L.; Figueiredo, J.L.; Silva, A.M.T. Prototype composite membranes of partially reduced graphene oxide/TiO₂ for photocatalytic ultrafiltration water treatment under visible light. *Appl. Catal. B Environ.* **2014**, *158–159*, 361–372. [[CrossRef](#)]

19. Anandan, S.; Narasinga Rao, T.; Sathish, M.; Rangappa, D.; Honma, I.; Miyauchi, M. Superhydrophilic graphene-loaded TiO₂ thin film for self-cleaning applications. *ACS Appl. Mater. Interfaces* **2013**, *5*, 207–212. [[CrossRef](#)] [[PubMed](#)]
20. Reutergårdh, L.B.; Ilangphasuk, M. Photocatalytic decolourization of reactive azo dye: A comparison between TiO₂ and us photocatalysis. *Chemosphere* **1997**, *35*, 585–596. [[CrossRef](#)]
21. Farghali, A.A.; Zaki, A.H.; Khedr, M.H. Control of Selectivity in Heterogeneous Photocatalysis by Tuning TiO₂ Morphology for Water Treatment Applications. *Nanomater. Nanotechnol.* **2016**, *6*, 12. [[CrossRef](#)]
22. Kalikeri, S.; Kamath, N.; Gadgil, D.J.; Shetty Kodialbail, V. Visible light-induced photocatalytic degradation of Reactive Blue-19 over highly efficient polyaniline-TiO₂ nanocomposite: A comparative study with solar and UV photocatalysis. *Environ. Sci. Pollut. Res.* **2017**, *25*, 3731–3744. [[CrossRef](#)] [[PubMed](#)]
23. Sornalingam, K.; McDonagh, A.; Zhou, J.L.; Johir, M.A.H.; Ahmed, M.B. Photocatalysis of estrone in water and wastewater: Comparison between Au-TiO₂ nanocomposite and TiO₂, and degradation by-products. *Sci. Total Environ.* **2018**, *610–611*, 521–530. [[CrossRef](#)] [[PubMed](#)]
24. Serna-Galvis, E.A.; Giraldo-Aguirre, A.L.; Silva-Agredo, J.; Flórez-Acosta, O.A.; Torres-Palma, R.A. Removal of antibiotic cloxacillin by means of electrochemical oxidation, TiO₂ photocatalysis, and photo-Fenton processes: Analysis of degradation pathways and effect of the water matrix on the elimination of antimicrobial activity. *Environ. Sci. Pollut. Res.* **2017**, *24*, 6339–6352. [[CrossRef](#)] [[PubMed](#)]
25. He, Y.; Sutton, N.B.; Rijnaarts, H.H.H.; Langenhoff, A.A.M. Degradation of pharmaceuticals in wastewater using immobilized TiO₂ photocatalysis under simulated solar irradiation. *Appl. Catal. B Environ.* **2016**, *182*, 132–141. [[CrossRef](#)]
26. Barndök, H.; Hermosilla, D.; Han, C.; Dionysiou, D.D.; Negro, C.; Blanco, Á. Degradation of 1,4-dioxane from industrial wastewater by solar photocatalysis using immobilized NF-TiO₂ composite with monodisperse TiO₂ nanoparticles. *Appl. Catal. B Environ.* **2016**, *180*, 44–52. [[CrossRef](#)]
27. Abeledo-Lameiro, M.J.; Reboredo-Fernández, A.; Polo-López, M.I.; Fernández-Ibáñez, P.; Ares-Mazás, E.; Gómez-Couso, H. Photocatalytic inactivation of the waterborne protozoan parasite *Cryptosporidium parvum* using TiO₂/H₂O₂ under simulated and natural solar conditions. *Catal. Today* **2017**, *280*, 132–138. [[CrossRef](#)]
28. Abeledo-Lameiro, M.J.; Ares-Mazás, E.; Gómez-Couso, H. Evaluation of solar photocatalysis using TiO₂ slurry in the inactivation of *Cryptosporidium parvum* oocysts in water. *J. Photochem. Photobiol. B Biol.* **2016**, *163*, 92–99. [[CrossRef](#)] [[PubMed](#)]
29. Sreeja, S.; Vidya Shetty, K. Microbial disinfection of water with endotoxin degradation by photocatalysis using Ag@TiO₂ core shell nanoparticles. *Environ. Sci. Pollut. Res.* **2016**, *23*, 18154–18164. [[CrossRef](#)]
30. Ye, M.; Jia, J.; Wu, Z.; Qian, C.; Chen, R.; O'Brien, P.G.; Sun, W.; Dong, Y.; Ozin, G.A. Synthesis of Black TiO_x Nanoparticles by Mg Reduction of TiO₂ Nanocrystals and their Application for Solar Water Evaporation. *Adv. Energy Mater.* **2017**, *7*, 1601811. [[CrossRef](#)]
31. Fan, C.; Chen, C.; Wang, J.; Fu, X.; Ren, Z.; Qian, G.; Wang, Z. Black Hydroxylated Titanium Dioxide Prepared via Ultrasonication with Enhanced Photocatalytic Activity. *Sci. Rep.* **2015**, *5*, 11712. [[CrossRef](#)] [[PubMed](#)]
32. Zimbone, M.; Cacciato, G.; Sanz, R.; Carles, R.; Gulino, A.; Privitera, V.; Grimaldi, M.G. Black TiO_x photocatalyst obtained by laser irradiation in water. *Catal. Commun.* **2016**, *84*, 11–15. [[CrossRef](#)]
33. Lin, L.; Huang, J.; Li, X.; Abass, M.A.; Zhang, S. Effective surface disorder engineering of metal oxide nanocrystals for improved photocatalysis. *Appl. Catal. B Environ.* **2017**, *203*, 615–624. [[CrossRef](#)]
34. Ullattil, S.G.; Narendranath, S.B.; Pillai, S.C.; Periyat, P. Black TiO₂ Nanomaterials: A Review of Recent Advances. *Chem. Eng. J.* **2018**, *343*, 708–736. [[CrossRef](#)]
35. Chen, X.; Zhao, D.; Liu, K.; Wang, C.; Liu, L.; Li, B.; Zhang, Z.; Shen, D. Laser-Modified Black Titanium Oxide Nanospheres and Their Photocatalytic Activities under Visible Light. *ACS Appl. Mater. Interfaces* **2015**, *7*, 16070–16077. [[CrossRef](#)] [[PubMed](#)]
36. Liu, Y.; Tian, L.; Tan, X.; Li, X.; Chen, X. Synthesis, properties, and applications of black titanium dioxide nanomaterials. *Sci. Bull.* **2017**, *62*, 431–441. [[CrossRef](#)]
37. Coto, M.; Divitini, G.; Dey, A.; Krishnamurthy, S.; Ullah, N.; Ducati, C.; Kumar, R.V. Tuning the properties of a black TiO₂-Ag visible light photocatalyst produced by a rapid one-pot chemical reduction. *Mater. Today Chem.* **2017**, *4*, 142–149. [[CrossRef](#)]
38. Ryu, J.; Choi, W. Substrate-Specific Photocatalytic Activities of TiO₂ and Multiactivity Test for Water Treatment Application. *Environ. Sci. Technol.* **2008**, *42*, 294–300. [[CrossRef](#)] [[PubMed](#)]

39. Minella, M.; Bertaina, F.; Minero, C. The complex interplay between adsorption and photoactivity in hybrids rGO/TiO₂. *Catal. Today* **2018**, *315*, 9–18. [[CrossRef](#)]
40. Khaki, M.D.; Shafeeyan, M.S.; Raman, A.A.; Daud, W.W. Application of doped photocatalysts for organic pollutant degradation—A review. *J. Environ. Manag.* **2017**, *198*, 78–94. [[CrossRef](#)] [[PubMed](#)]
41. Hashimoto, K.; Irie, H.; Fujishima, A. Photocatalysis: A Historical Overview and Future Prospects. *Jpn. J. Appl. Phys.* **2005**, *44*, 8269–8285. [[CrossRef](#)]
42. Farhangi, N. Nano TiO₂/Graphene Composites for Photovoltaic and Photocatalytic Materials. Ph.D. Thesis, University of Western Ontario, London, ON, Canada, 2012.
43. Hurtado, C.; Azucena, S.; Duarte, G. Effect of the synthesis variables of TiO₂ on the photocatalytic activity towards the degradation of water pollutants. *Revista de la Facultad de Ingeniería Universidad de Antioquia* **2011**, *57*, 49–56.
44. Wu, H.; Fan, J.; Liu, E.; Hu, X.; Ma, Y.; Fan, X.; Li, Y.; Tang, C. Facile hydrothermal synthesis of TiO₂ nanospindles-reduced graphene oxide composite with a enhanced photocatalytic activity. *J. Alloys Compd.* **2015**, *623*, 298–303. [[CrossRef](#)]
45. Sclafani, A.; Herrmann, J.M. Comparison of the Photoelectronic and Photocatalytic Activities of Various Anatase and Rutile Forms of Titania in Pure Liquid Organic Phases and in Aqueous Solutions. *J. Phys. Chem.* **1996**, *100*, 13655–13661. [[CrossRef](#)]
46. Fox, M.A.; Dulay, M.T. Heterogeneous photocatalysis. *Chem. Rev.* **1993**, *93*, 341–357. [[CrossRef](#)]
47. Wang, H.; Yuan, X.; Wu, Y.; Huang, H.; Peng, X.; Zeng, G.; Zhong, H.; Liang, J.; Ren, M.M. Graphene-based materials: Fabrication, characterization and application for the decontamination of wastewater and wastegas and hydrogen storage/generation. *Adv. Colloid Interface Sci.* **2013**, *195–196*, 19–40. [[CrossRef](#)] [[PubMed](#)]
48. Jiang, B.; Tian, C.; Pan, Q.; Jiang, Z.; Wang, J.-Q.; Yan, W.; Fu, H. Enhanced Photocatalytic Activity and Electron Transfer Mechanisms of Graphene/TiO₂ with Exposed {001} Facets. *J. Phys. Chem. C* **2011**, *115*, 23718–23725. [[CrossRef](#)]
49. Wang, Z.-C.; Shui, H.-F. Effect of PO₄³⁻ and PO₄³⁻-SO₄²⁻ modification of TiO₂ on its photocatalytic properties. *J. Mol. Catal. A Chem.* **2007**, *263*, 20–25. [[CrossRef](#)]
50. Bhanvase, B.A.; Shende, T.P.; Sonawane, S.A. review on graphene-TiO₂ and doped graphene-TiO₂ nanocomposite photocatalyst for water and wastewater treatment. *Environ. Technol. Rev.* **2017**, *6*, 1–14. [[CrossRef](#)]
51. Lin, L.; Wang, H.; Jiang, W.; Mkaouar, A.R.; Xu, P. Comparison study on photocatalytic oxidation of pharmaceuticals by TiO₂-Fe and TiO₂-reduced graphene oxide nanocomposites immobilized on optical fibers. *J. Hazard. Mater.* **2017**, *333*, 162–168. [[CrossRef](#)] [[PubMed](#)]
52. Tan, L.L.; Ong, W.J.; Chai, S.P.; Mohamed, A.R. Noble metal modified reduced graphene oxide/TiO₂ ternary nanostructures for efficient visible-light-driven photoreduction of carbon dioxide into methane. *Appl. Catal. B Environ.* **2015**, *166–167*, 251–259. [[CrossRef](#)]
53. Sohn, Y.; Huang, W.; Taghipour, F. Recent progress and perspectives in the photocatalytic CO₂ reduction of Ti-oxide-based nanomaterials. *Appl. Surf. Sci.* **2017**, *396*, 1696–1711. [[CrossRef](#)]
54. Low, J.; Cheng, B.; Yu, J. Surface modification and enhanced photocatalytic CO₂ reduction performance of TiO₂: A review. *Appl. Surf. Sci.* **2017**, *392*, 658–686. [[CrossRef](#)]
55. Ribao, P.; Rivero, M.J.; Ortiz, I. TiO₂ structures doped with noble metals and/or graphene oxide to improve the photocatalytic degradation of dichloroacetic acid. *Environ. Sci. Pollut. Res.* **2017**, *24*, 12628–12637. [[CrossRef](#)] [[PubMed](#)]
56. Liu, L.; Luo, C.; Xiong, J.; Yang, Z.; Zhang, Y.; Cai, Y.; Gu, H. Reduced graphene oxide (rGO) decorated TiO₂ microspheres for visible-light photocatalytic reduction of Cr(VI). *J. Alloys Compd.* **2017**, *690*, 771–776. [[CrossRef](#)]
57. Ghasemi, S.; Hashemian, S.J.; Alamolhoda, A.A.; Gocheva, I.; Rahman Setayesh, S. Plasmon enhanced photocatalytic activity of Au@TiO₂-graphene nanocomposite under visible light for degradation of pollutants. *Mater. Res. Bull.* **2017**, *87*, 40–47. [[CrossRef](#)]
58. Li, W.; Wang, F.; Liu, Y.; Wang, J.; Yang, J.; Zhang, L.; Elzatahry, A.A.; Aldhayan, D.M.; Xia, Y.; Zhao, D. General Strategy to Synthesize Uniform Mesoporous TiO₂/Graphene/Mesoporous TiO₂ Sandwich-Like Nanosheets for Highly Reversible Lithium Storage. *Nano Lett.* **2015**, *15*, 2186–2193. [[CrossRef](#)] [[PubMed](#)]

59. Rahimi, R.; Zargari, S.; Yousefi, A.; Yaghoubi Berijani, M.; Ghaffarinejad, A.; Morsali, A. Visible light photocatalytic disinfection of *E. coli* with TiO₂-graphene nanocomposite sensitized with tetrakis(4-carboxyphenyl)porphyrin. *Appl. Surf. Sci.* **2015**, *355*, 1098–1106. [CrossRef]
60. Khanna, A.; Shetty, K.V. Solar photocatalysis for treatment of Acid Yellow-17 (AY-17) dye contaminated water using Ag@TiO₂ core-shell structured nanoparticles. *Environ. Sci. Pollut. Res.* **2013**, *20*, 5692–5707. [CrossRef] [PubMed]
61. Ziyilan-Yavas, A.; Mizukoshi, Y.; Maeda, Y.; Ince, N.H. Supporting of pristine TiO₂ with noble metals to enhance the oxidation and mineralization of paracetamol by sonolysis and sonophotolysis. *Appl. Catal. B Environ.* **2015**, *172–173*, 7–17. [CrossRef]
62. Wu, S.; Jia, Q.; Dai, W. Synthesis of RGO/TiO₂ hybrid as a high performance photocatalyst. *Ceram. Int.* **2017**, *43*, 1530–1535. [CrossRef]
63. Graphene. Available online: <https://www.nobelprize.org/uploads/2018/06/advanced-physicsprize2010.pdf> (accessed on 23 October 2018).
64. Singh, V.; Joung, D.; Zhai, L.; Das, S.; Khondaker, S.I.; Seal, S. Graphene based materials: Past, present and future. *Prog. Mater. Sci.* **2011**, *56*, 1178–1271. [CrossRef]
65. Geim, A.K.; Novoselov, K.S. The rise of graphene. *Nat. Mater.* **2007**, *6*, 183–191. [CrossRef] [PubMed]
66. Chen, D.; Feng, H.; Li, J. Graphene oxide: Preparation, functionalization, and electrochemical applications. *Chem. Rev.* **2012**, *112*, 6027–6053. [CrossRef] [PubMed]
67. Zhu, Y.; Murali, S.; Cai, W.; Li, X.; Suk, J.W.; Potts, J.R.; Ruoff, R.S. Graphene and graphene oxide: Synthesis, properties, and applications. *Adv. Mater.* **2010**, *22*, 3906–3924. [CrossRef] [PubMed]
68. Dreyer, D.R.; Park, S.; Bielawski, C.W.; Ruoff, R.S. The chemistry of graphene oxide. *Chem. Soc. Rev.* **2010**, *39*, 228–240. [CrossRef] [PubMed]
69. Houas, A.; Lachheb, H.; Ksibi, M.; Elaloui, E.; Guillard, C. Photocatalytic degradation pathway of methylene blue in water. *Appl. Catal. B Environ.* **2001**, *31*, 145–157. [CrossRef]
70. Chowdhury, S.; Balasubramanian, R. Graphene/semiconductor nanocomposites (GSNs) for heterogeneous photocatalytic decolorization of wastewaters contaminated with synthetic dyes: A review. *Appl. Catal. B Environ.* **2014**, *160–161*, 307–324. [CrossRef]
71. Zhang, H.; Lv, X.; Li, Y.; Wang, Y.; Li, J. P25-graphene composite as a high performance photocatalyst. *ACS Nano* **2010**, *4*, 380–386. [CrossRef] [PubMed]
72. Yoo, D.-H.; Cuong, T.V.; Pham, V.H.; Chung, J.S.; Khoa, N.T.; Kim, E.J.; Hahn, S.H. Enhanced photocatalytic activity of graphene oxide decorated on TiO₂ films under UV and visible irradiation. *Curr. Appl. Phys.* **2011**, *11*, 805–808. [CrossRef]
73. Liu, J.; Bai, H.; Wang, Y.; Liu, Z.; Zhang, X.; Sun, D.D. Self-assembling TiO₂ nanorods on large graphene oxide sheets at a two-phase interface and their anti-recombination in photocatalytic applications. *Adv. Funct. Mater.* **2010**, *20*, 4175–4181. [CrossRef]
74. Leary, R.; Westwood, A. Carbonaceous nanomaterials for the enhancement of TiO₂ photocatalysis. *Carbon* **2011**, *49*, 741–772. [CrossRef]
75. Tan, L.-L.; Chai, S.-P.; Mohamed, A.R. Synthesis and applications of graphene-based TiO₂ photocatalysts. *ChemSusChem* **2012**, *5*, 1868–1882. [CrossRef] [PubMed]
76. Zhao, D.; Sheng, G.; Chen, C.; Wang, X. Enhanced photocatalytic degradation of methylene blue under visible irradiation on graphene@TiO₂ dyade structure. *Appl. Catal. B Environ.* **2012**, *111–112*, 303–308. [CrossRef]
77. Xu, H.; Ouyang, S.; Liu, L.; Reunchan, P.; Umezawa, N.; Ye, J. Recent advances in TiO₂-based photocatalysis. *J. Mater. Chem. A* **2014**, *2*, 12642–12661. [CrossRef]
78. Dahl, M.; Liu, Y.; Yin, Y. Composite Titanium Dioxide Nanomaterials. *Chem. Rev.* **2014**, *114*, 9853–9889. [CrossRef] [PubMed]
79. Fang, W.; Xing, M.; Zhang, J. Modifications on reduced titanium dioxide photocatalysts: A review. *J. Photochem. Photobiol. C Photochem. Rev.* **2017**, *32*, 21–39. [CrossRef]
80. Upadhyay, R.K.; Sooin, N.; Roy, S.S. Role of graphene/metal oxide composites as photocatalysts, adsorbents and disinfectants in water treatment: A review. *RSC Adv.* **2014**, *4*, 3823–3851. [CrossRef]
81. Cao, Y.; Li, X. Adsorption of graphene for the removal of inorganic pollutants in water purification: A review. *Adsorption* **2014**, *20*, 713–727. [CrossRef]

82. Morales-Torres, S.; Pastrana-Martínez, L.M.; Figueiredo, J.L.; Faria, J.L.; Silva, A.M.T. Design of graphene-based TiO₂ photocatalysts—A review. *Environ. Sci. Pollut. Res.* **2012**, *19*, 3676–3687. [[CrossRef](#)] [[PubMed](#)]
83. Yu, X.; Lin, D.; Li, P.; Su, Z. Recent advances in the synthesis and energy applications of TiO₂-graphene nanohybrids. *Sol. Energy Mater. Sol. Cells* **2017**, *172*, 252–269. [[CrossRef](#)]
84. Faraldos, M.; Bahamonde, A. Environmental applications of titania-graphene photocatalysts. *Catal. Today* **2017**, *285*, 13–28. [[CrossRef](#)]
85. Cheetham, K. *The Chemistry of Nanomaterials: Synthesis, Properties and Applications*; Rao, C.N.R., Muller, A., Cheetham, A.K., Eds.; WILEY-VCH Verlag GmbH & Co. KGaA: Weinheim, Germany, 2004; ISBN 3527306862.
86. Chen, X.; Mao, S.S. Titanium dioxide nanomaterials: Synthesis, properties, modifications and applications. *Chem. Rev.* **2007**, *107*, 2891–2959. [[CrossRef](#)] [[PubMed](#)]
87. Guo, Z.; Tan, L. *Fundamentals and Applications of Nanomaterials*; Artech House: Washington, DC, USA, 2009; ISBN 1596932635.
88. Byrappa, K.; Yoshimura, M. *Handbook of Hydrothermal Technology: A Technology for Crystal Growth and Materials Processing*; McGuire, G.E., Rosnagel, S.M., Bunshah, R.F., Eds.; William Andrew Publishing: Norwich, NY, USA, 2001; ISBN 081551445X.
89. Sher Shah, M.S.A.; Park, R.; Zhang, K.; Park, J.H.; Yoo, P.J. Green synthesis of biphasic TiO₂-reduced graphene oxide nanocomposites with highly enhanced photocatalytic activity. *ACS Appl. Mater. Interfaces* **2012**, *4*, 3893–3901. [[CrossRef](#)] [[PubMed](#)]
90. Gu, Y.; Xing, M.; Zhang, J. Synthesis and photocatalytic activity of graphene based doped TiO₂ nanocomposites. *Appl. Surf. Sci.* **2014**, *319*, 2–9. [[CrossRef](#)]
91. Perera, S.D.; Mariano, R.G.; Vu, K.; Nour, N.; Seitz, O.; Chabal, Y.; Balkus, K.J. Hydrothermal Synthesis of Graphene-TiO₂ Nanotube Composites with Enhanced Photocatalytic Activity. *ACS Catal.* **2012**, *2*, 949–956. [[CrossRef](#)]
92. Pan, X.; Zhao, Y.; Wang, S.; Fan, Z. TiO₂/graphene nanocomposite for photocatalytic application. In *Materials and Processes for Energy: Communicating Current Research and Technological Developments*; Méndez-Vilas, A., Ed.; Formatex Research Center: Badajoz, Spain, 2013; pp. 913–920.
93. Bai, X.; Zhang, X.; Hua, Z.; Ma, W.; Dai, Z.; Huang, X.; Gu, H. Uniformly distributed anatase TiO₂ nanoparticles on graphene: Synthesis, characterization, and photocatalytic application. *J. Alloys Compd.* **2014**, *599*, 10–18. [[CrossRef](#)]
94. Li, J.; Zhou, S.L.; Hong, G.B.; Chang, C.T. Hydrothermal preparation of P25-graphene composite with enhanced adsorption and photocatalytic degradation of dyes. *Chem. Eng. J.* **2013**, *219*, 486–491. [[CrossRef](#)]
95. Shi, J.-W.; Ai, H.-Y.; Chen, J.-W.; Cui, H.-J.; Fu, M.-L. The composite of nitrogen-doped anatase titania plates with exposed {001} facets/graphene nanosheets for enhanced visible-light photocatalytic activity. *J. Colloid Interface Sci.* **2014**, *430*, 100–107. [[CrossRef](#)] [[PubMed](#)]
96. Lee, J.S.; You, K.H.; Park, C.B. Highly photoactive, low bandgap TiO₂ nanoparticles wrapped by graphene. *Adv. Mater.* **2012**, *24*, 1084–1088. [[CrossRef](#)] [[PubMed](#)]
97. Ni, Y.; Wang, W.; Huang, W.; Lu, C.; Xu, Z. Graphene strongly wrapped TiO₂ for high-reactive photocatalyst: A new sight for significant application of graphene. *J. Colloid Interface Sci.* **2014**, *428*, 162–169. [[CrossRef](#)] [[PubMed](#)]
98. Linley, S.; Liu, Y.; Ptacek, C.J.; Blowes, D.W.; Gu, F.X. Recyclable graphene oxide-supported titanium dioxide photocatalysts with tunable properties. *ACS Appl. Mater. Interfaces* **2014**, *6*, 4658–4668. [[CrossRef](#)] [[PubMed](#)]
99. Ariffin, S.N.; Lim, H.N.; Jumeri, F.A.; Zobir, M.; Abdullah, A.H.; Ahmad, M.; Ibrahim, N.A.; Huang, N.M.; Teo, P.S.; Muthoosamy, K.; et al. Modification of polypropylene filter with metal oxide and reduced graphene oxide for water treatment. *Ceram. Int.* **2014**, *40*, 6927–6936. [[CrossRef](#)]
100. Nguyen, P.T.N.; Salim, C.; Kurniawan, W.; Hinode, H. A non-hydrolytic sol-gel synthesis of reduced graphene oxide/TiO₂ microsphere photocatalysts. *Catal. Today* **2014**, *230*, 166–173. [[CrossRef](#)]
101. Kim, T.-W.; Park, M.; Kim, H.Y.; Park, S.-J. Preparation of flower-like TiO₂ sphere/reduced graphene oxide composites for photocatalytic degradation of organic pollutants. *J. Solid State Chem.* **2016**, *239*, 91–98. [[CrossRef](#)]
102. Zhang, Y.; Hou, X.; Sun, T.; Zhao, X. Calcination of reduced graphene oxide decorated TiO₂ composites for recovery and reuse in photocatalytic applications. *Ceram. Int.* **2017**, *43*, 1150–1159. [[CrossRef](#)]

103. Zhang, Z.; Xiao, F.; Guo, Y.; Wang, S.; Liu, Y. One-pot self-assembled three-dimensional TiO₂-graphene hydrogel with improved adsorption capacities and photocatalytic and electrochemical activities. *ACS Appl. Mater. Interfaces* **2013**, *5*, 2227–2233. [[CrossRef](#)] [[PubMed](#)]
104. Li, Y.; Yang, J.; Zheng, S.; Zeng, W.; Zhao, N.; Shen, M. One-pot synthesis of 3D TiO₂-reduced graphene oxide aerogels with superior adsorption capacity and enhanced visible-light photocatalytic performance. *Ceram. Int.* **2016**, *42*, 19091–19096. [[CrossRef](#)]
105. Men, X.; Wu, Y.; Chen, H.; Fang, X.; Sun, H.; Yin, S.; Qin, W. Facile fabrication of TiO₂/Graphene composite foams with enhanced photocatalytic properties. *J. Alloys Compd.* **2017**, *703*, 251–257. [[CrossRef](#)]
106. Pan, X.; Zhao, Y.; Liu, S.; Korzeniewski, C.L.; Wang, S.; Fan, Z. Comparing Graphene-TiO₂ Nanowire and Graphene-TiO₂ Nanoparticle Composite Photocatalysts. *ACS Appl. Mater. Interfaces* **2012**, *4*, 3944–3950. [[CrossRef](#)] [[PubMed](#)]
107. Najafi, M.; Kermanpur, A.; Rahimpour, M.R.; Najafzadeh, A. Effect of TiO₂ morphology on structure of TiO₂-graphene oxide nanocomposite synthesized via a one-step hydrothermal method. *J. Alloys Compd.* **2017**, *722*, 272–277. [[CrossRef](#)]
108. Safajou, H.; Khojasteh, H.; Salavati-Niasari, M.; Mortazavi-Derazkola, S. Enhanced photocatalytic degradation of dyes over graphene/Pd/TiO₂ nanocomposites: TiO₂ nanowires versus TiO₂ nanoparticles. *J. Colloid Interface Sci.* **2017**, *498*, 423–432. [[CrossRef](#)] [[PubMed](#)]
109. Shao, P.; Tian, J.; Shi, W.; Gao, S.; Cui, F. Eco-friendly one-pot synthesis of ultradispersed TiO₂ nanocrystals/graphene nanocomposites with high photocatalytic activity for dye degradation. *J. Mater. Chem. A Mater. Energy Sustain.* **2015**, *3*, 19913–19919. [[CrossRef](#)]
110. Qu, A.; Xie, H.; Xu, X.; Zhang, Y.; Wen, S.; Cui, Y. High quantum yield graphene quantum dots decorated TiO₂ nanotubes for enhancing photocatalytic activity. *Appl. Surf. Sci.* **2016**, *375*, 230–241. [[CrossRef](#)]
111. Min, S.; Hou, J.; Lei, Y.; Ma, X.; Lu, G. Facile one-step hydrothermal synthesis toward strongly coupled TiO₂/graphene quantum dots photocatalysts for efficient hydrogen evolution. *Appl. Surf. Sci.* **2017**, *396*, 1375–1382. [[CrossRef](#)]
112. Zhang, Y.; Qi, F.; Li, Y.; Zhou, X.; Sun, H.; Zhang, W.; Liu, D.; Song, X.M. Graphene oxide quantum dot-sensitized porous titanium dioxide microsphere: Visible-light-driven photocatalyst based on energy band engineering. *J. Colloid Interface Sci.* **2017**, *498*, 105–111. [[CrossRef](#)] [[PubMed](#)]
113. Safardoust-Hojaghan, H.; Salavati-Niasari, M. Degradation of methylene blue as a pollutant with N-doped graphene quantum dot/titanium dioxide nanocomposite. *J. Clean. Prod.* **2017**, *148*, 31–36. [[CrossRef](#)]
114. Tian, H.; Shen, K.; Hu, X.; Qiao, L.; Zheng, W. N, S co-doped graphene quantum dots-graphene-TiO₂ nanotubes composite with enhanced photocatalytic activity. *J. Alloys Compd.* **2017**, *691*, 369–377. [[CrossRef](#)]
115. Cai, D.; Lian, P.; Zhu, X.; Liang, S.; Yang, W.; Wang, H. High specific capacity of TiO₂-graphene nanocomposite as an anode material for lithium-ion batteries in an enlarged potential window. *Electrochim. Acta* **2012**, *74*, 65–72. [[CrossRef](#)]
116. Wang, C.; Cao, M.; Wang, P.; Ao, Y.; Hou, J.; Qian, J. Preparation of graphene-carbon nanotube-TiO₂ composites with enhanced photocatalytic activity for the removal of dye and Cr (VI). *Appl. Catal. A Gen.* **2014**, *473*, 83–89. [[CrossRef](#)]
117. Qian, W.; Greaney, P.A.; Fowler, S.; Chiu, S.; Goforth, A.M.; Jiao, J. Low-Temperature Nitrogen Doping in Ammonia Solution for Production of N-Doped TiO₂-Hybridized Graphene as a Highly Efficient Photocatalyst for Water Treatment. *ACS Sustain. Chem. Eng.* **2014**, *2*, 1802–1810. [[CrossRef](#)]
118. Li, K.; Xiong, J.; Chen, T.; Yan, L.; Dai, Y.; Song, D.; Lv, Y.; Zeng, Z. Preparation of graphene/TiO₂ composites by nonionic surfactant strategy and their simulated sunlight and visible light photocatalytic activity towards representative aqueous POPs degradation. *J. Hazard. Mater.* **2013**, *250–251*, 19–28. [[CrossRef](#)] [[PubMed](#)]
119. Huang, Q.; Tian, S.; Zeng, D.; Wang, X.; Song, W.; Li, Y.; Xiao, W.; Xie, C. Enhanced Photocatalytic Activity of Chemically Bonded TiO₂/Graphene Composites Based on the Effective Interfacial Charge Transfer through the C–Ti Bond. *ACS Catal.* **2013**, *3*, 1477–1485. [[CrossRef](#)]
120. Min, Y.; Zhang, K.; Zhao, W.; Zheng, F.; Chen, Y.; Zhang, Y. Enhanced chemical interaction between TiO₂ and graphene oxide for photocatalytic decolorization of methylene blue. *Chem. Eng. J.* **2012**, *193–194*, 203–210. [[CrossRef](#)]
121. Xie, Y.; Song, J.; Zhou, P.; Ling, Y.; Wu, Y. Controllable Synthesis of TiO₂/Graphene Nanocomposites for Long Lifetime Lithium Storage: Nanoparticles vs. Nanolayers. *Electrochim. Acta* **2016**, *210*, 358–366. [[CrossRef](#)]

122. Gu, L.; Wang, J.; Cheng, H.; Zhao, Y.; Liu, L.; Han, X. One-step preparation of graphene-supported anatase TiO₂ with exposed {001} facets and mechanism of enhanced photocatalytic properties. *ACS Appl. Mater. Interfaces* **2013**, *5*, 3085–3093. [[CrossRef](#)] [[PubMed](#)]
123. Morales-Torres, S.; Pastrana-Martínez, L.M.; Figueiredo, J.L.; Faria, J.L.; Silva, A.M.T. Graphene oxide-P25 photocatalysts for degradation of diphenhydramine pharmaceutical and methyl orange dye. *Appl. Surf. Sci.* **2013**, *275*, 361–368. [[CrossRef](#)]
124. Gao, P.; Li, A.; Sun, D.D.; Ng, W.J. Effects of various TiO₂ nanostructures and graphene oxide on photocatalytic activity of TiO₂. *J. Hazard. Mater.* **2014**, *279*, 96–104. [[CrossRef](#)] [[PubMed](#)]
125. Liu, J.; Liu, L.; Bai, H.; Wang, Y.; Sun, D.D. Gram-scale production of graphene oxide-TiO₂ nanorod composites: Towards high-activity photocatalytic materials. *Appl. Catal. B Environ.* **2011**, *106*, 76–82. [[CrossRef](#)]
126. Nguyen-Phan, T.D.; Pham, V.H.; Shin, E.W.; Pham, H.D.; Kim, S.; Chung, J.S.; Kim, E.J.; Hur, S.H. The role of graphene oxide content on the adsorption-enhanced photocatalysis of titanium dioxide/graphene oxide composites. *Chem. Eng. J.* **2011**, *170*, 226–232. [[CrossRef](#)]
127. Thomas, R.T.; Abdul Rasheed, P.; Sandhyarani, N. Synthesis of nanotitania decorated few-layer graphene for enhanced visible light driven photocatalysis. *J. Colloid Interface Sci.* **2014**, *428*, 214–221. [[CrossRef](#)] [[PubMed](#)]
128. Pu, S.; Zhu, R.; Ma, H.; Deng, D.; Pei, X.; Qi, F.; Chu, W. Facile in-situ design strategy to disperse TiO₂ nanoparticles on graphene for the enhanced photocatalytic degradation of rhodamine 6G. *Appl. Catal. B Environ.* **2017**, *218*, 208–219. [[CrossRef](#)]
129. Kim, H.I.; Moon, G.H.; Monllor-Satoca, D.; Park, Y.; Choi, W. Solar photoconversion using graphene/TiO₂ composites: Nanographene shell on TiO₂ core versus TiO₂ nanoparticles on graphene sheet. *J. Phys. Chem. C* **2012**, *116*, 1535–1543. [[CrossRef](#)]
130. Bell, N.J.; Ng, Y.H.; Du, A.; Coster, H.; Smith, S.C.; Amal, R. Understanding the Enhancement in Photoelectrochemical Properties of Photocatalytically Prepared TiO₂-Reduced Graphene Oxide Composite. *J. Phys. Chem. C* **2011**, *115*, 6004–6009. [[CrossRef](#)]
131. Brinker, C.; Scherer, G. *Sol-Gel Science The Physics and Chemistry of Sol-Gel Processing*; Academic Press: London, UK, 1990.
132. Hamadani, M.; Rostami, M.; Jabbari, V. Graphene-supported C–N–S tridoped TiO₂ photo-catalyst with improved band gap and charge transfer properties. *J. Mater. Sci. Mater. Electron.* **2017**, *28*, 15637–15646. [[CrossRef](#)]
133. Zhang, X.-Y.; Li, H.-P.; Cui, X.-L.; Lin, Y. Graphene/TiO₂ nanocomposites: Synthesis, characterization and application in hydrogen evolution from water photocatalytic splitting. *J. Mater. Chem.* **2010**, *20*, 2801–2806. [[CrossRef](#)]
134. Liu, S.S.; Sun, H.; Liu, S.S.; Wang, S. Graphene facilitated visible light photodegradation of methylene blue over titanium dioxide photocatalysts. *Chem. Eng. J.* **2013**, *214*, 298–303. [[CrossRef](#)]
135. Park, C.Y.; Kefayat, U.; Vikram, N.; Ghosh, T.; Oh, W.C.; Cho, K.Y. Preparation of novel CdS-graphene/TiO₂ composites with high photocatalytic activity for methylene blue dye under visible light. *Bull. Mater. Sci.* **2013**, *36*, 869–876. [[CrossRef](#)]
136. Niesen, T.P.; Guire, M.R. Review: Deposition of Ceramic Thin Films at Low Temperatures from Aqueous Solutions. *J. Electroceram.* **2001**, *6*, 169–207. [[CrossRef](#)]
137. Pastrana-Martínez, L.M.; Morales-Torres, S.; Likodimos, V.; Figueiredo, J.L.; Faria, J.L.; Falaras, P.; Silva, A.M.T. Advanced nanostructured photocatalysts based on reduced graphene oxide-TiO₂ composites for degradation of diphenhydramine pharmaceutical and methyl orange dye. *Appl. Catal. B Environ.* **2012**, *123–124*, 241–256. [[CrossRef](#)]
138. Pastrana-Martínez, L.M.; Morales-Torres, S.; Kontos, A.G.; Moustakas, N.G.; Faria, J.L.; Doña-Rodríguez, J.M.; Falaras, P.; Silva, A.M.T. TiO₂, surface modified TiO₂ and graphene oxide-TiO₂ photocatalysts for degradation of water pollutants under near-UV/Vis and visible light. *Chem. Eng. J.* **2013**, *224*, 17–23. [[CrossRef](#)]
139. Jiang, G.; Lin, Z.; Chen, C.; Zhu, L.; Chang, Q.; Wang, N.; Wei, W.; Tang, H. TiO₂ nanoparticles assembled on graphene oxide nanosheets with high photocatalytic activity for removal of pollutants. *Carbon* **2011**, *49*, 2693–2701. [[CrossRef](#)]
140. Zhang, N.; Li, B.; Li, S.; Yang, S. Graphene-supported mesoporous titania nanosheets for efficient photodegradation. *J. Colloid Interface Sci.* **2017**, *505*, 711–718. [[CrossRef](#)] [[PubMed](#)]

141. Xu, C.; Xu, Y.; Zhu, J. Photocatalytic Antifouling Graphene Oxide-Mediated Hierarchical Filtration Membranes with Potential Applications on Water Purification. *ACS Appl. Mater. Interfaces* **2014**, *6*, 16117–16123. [CrossRef] [PubMed]
142. Pham, D.K.; Horing, N.; Fritsching, U.; Madler, L. Highly Porous Film Synthesis by Single-Step Direct Aerosol Deposition. *Eurozoru Kenkyu* **2010**, *25*, 140–148.
143. Park, J.-J.; Lee, J.-G.; Kim, D.-Y.; Hong, J.-H.; Kim, J.-J.; Hong, S.; Yoon, S.S. Antibacterial and water purification activities of self-assembled honeycomb structure of aerosol deposited titania film. *Environ. Sci. Technol.* **2012**, *46*, 12510–12518. [CrossRef] [PubMed]
144. Kim, D.-Y.; Joshi, B.N.; Park, J.-J.; Lee, J.-G.; Cha, Y.-H.; Seong, T.-Y.; Noh, S.I.; Ahn, H.-J.; Al-Deyabe, S.S.; Yoon, S.S. Graphene–titania films by supersonic kinetic spraying for enhanced performance of dye-sensitized solar cells. *Ceram. Int.* **2014**, *40*, 11089–11097. [CrossRef]
145. Qin, H.; Xu, Y.; Kim, J.; Hwang, T.; Kim, T. The effect of structure on the photoactivity of a graphene/TiO₂ composite. *Mater. Sci. Eng. B Solid-State Mater. Adv. Technol.* **2014**, *184*, 72–79. [CrossRef]
146. Wojtoniszak, M.; Dolat, D.; Morawski, A.; Mijowska, E. Carbon-modified TiO₂ for photocatalysis. *Nanoscale Res. Lett.* **2012**, *7*, 235. [CrossRef] [PubMed]
147. Gao, Y.; Hu, M.; Mi, B. Membrane surface modification with TiO₂-graphene oxide for enhanced photocatalytic performance. *J. Membr. Sci.* **2014**, *455*, 349–356. [CrossRef]
148. Yang, Y.; Liu, E.; Fan, J.; Hu, X.; Hou, W.; Wu, F.; Ma, Y. Green and facile microwave-assisted synthesis of TiO₂/graphene nanocomposite and their photocatalytic activity for methylene blue degradation. *Russ. J. Phys. Chem. A* **2014**, *88*, 478–483. [CrossRef]
149. Shanmugam, M.; Alsalmeh, A.; Alghamdi, A.; Jayavel, R. In-situ microwave synthesis of graphene-TiO₂ nanocomposites with enhanced photocatalytic properties for the degradation of organic pollutants. *J. Photochem. Photobiol. B Biol.* **2016**, *163*, 216–223. [CrossRef] [PubMed]
150. Peining, Z.; Nair, A.S.; Shengjie, P.; Shengyuan, Y.; Ramakrishna, S. Facile fabrication of TiO₂-graphene composite with enhanced photovoltaic and photocatalytic properties by electrospinning. *ACS Appl. Mater. Interfaces* **2012**, *4*, 581–585. [CrossRef]
151. Kalantar-zadeh, K.; Fry, B. Chapter 5: Characterization Techniques for Nanomaterials. In *Nanotechnology-Enabled Sensors*; Springer: Berlin/Heidelberg, Germany, 2008; pp. 211–281.
152. Basheer, C. Application of titanium dioxide-graphene composite material for photocatalytic degradation of alkylphenols. *J. Chem.* **2013**, *2013*, 1–10. [CrossRef]
153. Egerton, R.F. Operating Principle of the SEM. In *Physical Principles of Electron Microscopy*; Springer: New York, NY, USA, 2005; pp. 125–153. ISBN 978-0-387-26016-7.
154. Transmission Electron Microscope (TEM)—Uses, Advantages and Disadvantages. Available online: <http://www.microscopemaster.com/transmission-electron-microscope.html> (accessed on 26 February 2015).
155. Egerton, R. The Transmission Electron Microscope. In *Physical Principles of Electron Microscopy: An Introduction to TEM, SEM, and AEM*; Springer: New York, NY, USA, 2005; pp. 57–92.
156. Brunauer, S.; Emmett, P.H.; Teller, E. Adsorption of Gases in Multimolecular Layers. *J. Am. Chem. Soc.* **1938**, *60*, 309–319. [CrossRef]
157. Brunauer, S. *The Adsorption of Gases and Vapors. Physical Adsorption*; Princeton University Press: Princeton, NJ, USA, 1943; Volume 1, ISBN 1443727369.
158. Pastrana-Martínez, L.M.; Morales-Torres, S.; Likodimos, V.; Falaras, P.; Figueiredo, J.L.; Faria, J.L.; Silva, A.M.T. Role of oxygen functionalities on the synthesis of photocatalytically active graphene-TiO₂ composites. *Appl. Catal. B Environ.* **2014**, *158–159*, 329–340. [CrossRef]
159. Myrick, M.L.; Simcock, M.N.; Baranowski, M.; Brooke, H.; Morgan, S.L.M. The Kubelka-Munk Diffuse Reflectance Formula Revisited. *Appl. Spectrosc. Rev.* **2011**, *46*, 140–165. [CrossRef]
160. Sun, H.; Liu, S.S.; Liu, S.S.; Wang, S. A comparative study of reduced graphene oxide modified TiO₂, ZnO and Ta₂O₅ in visible light photocatalytic/photochemical oxidation of methylene blue. *Appl. Catal. B Environ.* **2014**, *146*, 162–168. [CrossRef]
161. Fan, W.; Lai, Q.; Zhang, Q.; Wang, Y. Nanocomposites of TiO₂ and reduced graphene oxide as efficient photocatalysts for hydrogen evolution. *J. Phys. Chem. C* **2011**, *115*, 10694–10701. [CrossRef]
162. Tan, L.-L.; Ong, W.-J.; Chai, S.-P.; Mohamed, A.R. Reduced graphene oxide-TiO₂ nanocomposite as a promising visible-light-active photocatalyst for the conversion of carbon dioxide. *Nanoscale Res. Lett.* **2013**, *8*, 465. [CrossRef] [PubMed]

163. Qiu, J.; Zhang, P.; Ling, M.; Li, S.; Liu, P.; Zhao, H.; Zhang, S. Photocatalytic synthesis of TiO₂ and reduced graphene oxide nanocomposite for lithium ion battery. *ACS Appl. Mater. Interfaces* **2012**, *4*, 3636–3642. [[CrossRef](#)] [[PubMed](#)]
164. Hu, S.; Li, F.; Fan, Z. The Property and Photocatalytic Performance Comparison of Graphene, Carbon Nanotube, and C₆₀ Modified TiO₂ Nanocomposite Photocatalysts. *Bull. Korean Chem. Soc.* **2013**, *34*, 3671–3676. [[CrossRef](#)]
165. Muthirulan, P.; Devi, C.K.N.; Sundaram, M.M. Fabrication and characterization of efficient hybrid photocatalysts based on titania and graphene for acid orange seven dye degradation under UV irradiation. *Adv. Mater. Lett.* **2014**, *5*, 163–171. [[CrossRef](#)]
166. Huang, X.; Wang, L.; Zhou, J.; Gao, N. Photocatalytic decomposition of bromate ion by the UV/P25-Graphene processes. *Water Res.* **2014**, *57*, 1–7. [[CrossRef](#)] [[PubMed](#)]
167. Hao, X.; Jin, Z.; Xu, J.; Min, S.; Lu, G. Functionalization of TiO₂ with graphene quantum dots for efficient photocatalytic hydrogen evolution. *Superlattices Microstruct.* **2016**, *94*, 237–244. [[CrossRef](#)]
168. Harvey, D. Spectroscopic Methods. In *Modern Analytical Chemistry*; McGraw-Hill Companies: New York, NY, USA, 2008; pp. 543–666. ISBN 0-07-237547-7.
169. Hofmann, A. 12 Spectroscopic techniques: I Spectrophotometric techniques. In *Principles and Techniques of Biochemistry and Molecular Biology*; Wilson, K., Walker, J., Eds.; Cambridge University Press: Cambridge, UK, 2010; pp. 477–521.
170. Kusiak-Nejman, E.; Wanag, A.; Kowalczyk, Ł.; Kapica-Kozar, J.; Colbeau-Justin, C.; Mendez Medrano, M.G.; Morawski, A.W. Graphene oxide-TiO₂ and reduced graphene oxide-TiO₂ nanocomposites: Insight in charge-carrier lifetime measurements. *Catal. Today* **2017**, *287*, 189–195. [[CrossRef](#)]
171. Wang, J.; Wang, P.; Cao, Y.; Chen, J.; Li, W.; Shao, Y.; Zheng, Y.; Li, D. A high efficient photocatalyst Ag₃VO₄/TiO₂/graphene nanocomposite with wide spectral response. *Appl. Catal. B Environ.* **2013**, *136–137*, 94–102. [[CrossRef](#)]
172. Spange, S.; Prause, S.; Vilsmeier, E.; Thiel, W.R. Probing surface basicity of solid acids with an aminobenzodifurandione dye as the solvatochromic probe. *J. Phys. Chem. B* **2005**, *109*, 7280–7289. [[CrossRef](#)] [[PubMed](#)]
173. Park, Y.; Kim, W.; Park, H.; Tachikawa, T.; Majima, T.; Choi, W. Carbon-doped TiO₂ photocatalyst synthesized without using an external carbon precursor and the visible light activity. *Appl. Catal. B Environ.* **2009**, *91*, 355–361. [[CrossRef](#)]
174. El Seoud, O.A.; Ramadan, A.R.; Sato, B.M.; Pires, P.A.R. Surface properties of calcinated titanium dioxide probed by solvatochromic indicators: Relevance to catalytic applications. *J. Phys. Chem. C* **2010**, *114*, 10436–10443. [[CrossRef](#)]
175. Thielmann, F. Introduction into the characterisation of porous materials by inverse gas chromatography. *J. Chromatogr. A* **2004**, *1037*, 115–123. [[CrossRef](#)] [[PubMed](#)]
176. Voelkel, A.; Strzemiecka, B.; Adamska, K.; Milczewska, K. Inverse gas chromatography as a source of physiochemical data. *J. Chromatogr. A* **2009**, *1216*, 1551–1566. [[CrossRef](#)] [[PubMed](#)]
177. Dai, J.-F.; Wang, G.-J.; Wu, C.-K. Investigation of the Surface Properties of Graphene Oxide and Graphene by Inverse Gas Chromatography. *Chromatographia* **2014**, *77*, 299–307. [[CrossRef](#)]
178. Tayel, A.; Ramadan, A.R.; El Seoud, O.A. Variation of Surface Properties of Ceramic and Composite Nanostructures and their Measurements by a Novel Approach using Perichromic Dyes. Master's Thesis, The American University in Cairo, New Cairo, Egypt, 2015.
179. Rahman, M.A.; Amin, S.M.R.; Alam, M.S. Removal of Methylene Blue from Waste Water Using Activated Carbon Prepared from Rice Husk. *Dhaka Univ. J. Sci.* **2012**, *60*, 185–189. [[CrossRef](#)]
180. Zita, J.; Krýsa, J.; Mills, A. Correlation of oxidative and reductive dye bleaching on TiO₂ photocatalyst films. *J. Photochem. Photobiol. A Chem.* **2009**, *203*, 119–124. [[CrossRef](#)]
181. Gan, Z.; Wu, X.; Meng, M.; Zhu, X.; Yang, L.; Chu, P.K. Photothermal Contribution to Enhanced Photocatalytic Performance. *ACS Nano* **2014**, *8*, 9304–9310. [[CrossRef](#)] [[PubMed](#)]
182. Alamelu, K.; Raja, V.; Shiamala, L.; Jaffar Ali, B.M. Biphasic TiO₂ nanoparticles decorated graphene nanosheets for visible light driven photocatalytic degradation of organic dyes. *Appl. Surf. Sci.* **2018**, *430*, 145–154. [[CrossRef](#)]
183. Liang, Y.; Wang, H.; Casalongue, H.S.; Chen, Z.; Dai, H. TiO₂ Nanocrystals grown on graphene as advanced photocatalytic hybrid materials. *Nano Res.* **2010**, *3*, 701–705. [[CrossRef](#)]

184. Amalraj Appavoo, I.; Hu, J.; Huang, Y.; Li, S.F.Y.; Ong, S.L. Response surface modeling of Carbamazepine (CBZ) removal by Graphene-P25 nanocomposites/UVA process using central composite design. *Water Res.* **2014**, *57*, 270–279. [CrossRef] [PubMed]
185. Nawaz, M.; Miran, W.; Jang, J.; Lee, D.S. One-step hydrothermal synthesis of porous 3D reduced graphene oxide/TiO₂ aerogel for carbamazepine photodegradation in aqueous solution. *Appl. Catal. B Environ.* **2017**, *203*, 85–95. [CrossRef]
186. Lin, L.; Wang, H.; Xu, P. Immobilized TiO₂-reduced graphene oxide nanocomposites on optical fibers as high performance photocatalysts for degradation of pharmaceuticals. *Chem. Eng. J.* **2017**, *310*, 389–398. [CrossRef]
187. Cruz, M.; Gomez, C.; Duran-Valle, C.J.; Pastrana-Martínez, L.M.; Faria, J.L.; Silva, A.M.T.; Faraldos, M.; Bahamonde, A. Bare TiO₂ and graphene oxide TiO₂ photocatalysts on the degradation of selected pesticides and influence of the water matrix. *Appl. Surf. Sci.* **2017**, *416*, 1013–1021. [CrossRef]
188. Yu, Y.; Yan, L.; Cheng, J.; Jing, C. Mechanistic insights into TiO₂ thickness in Fe₃O₄@TiO₂-GO composites for enrofloxacin photodegradation. *Chem. Eng. J.* **2017**, *325*, 647–654. [CrossRef]
189. Gholamvande, Z.; Morrissey, A.; Nolan, K.; Tobin, J. Graphene/TiO₂ Nano-Composite for Photocatalytic Removal of Pharmaceuticals from Water. Available online: http://keynote.conference-services.net/resources/444/2653/pdf/iwawce2012_0244.pdf (accessed on 14 January 2016).
190. Calza, P.; Hadjicostas, C.; Sakkas, V.A.; Sarro, M.; Minero, C.; Medana, C.; Albanis, T.A. Photocatalytic transformation of the antipsychotic drug risperidone in aqueous media on reduced graphene oxide-TiO₂ composites. *Appl. Catal. B Environ.* **2016**, *183*, 96–106. [CrossRef]
191. Li, Z.; Qi, M.; Tu, C.; Wang, W.; Chen, J.; Wang, A.-J. Highly efficient removal of chlorotetracycline from aqueous solution using graphene oxide/TiO₂ composite: Properties and mechanism. *Appl. Surf. Sci.* **2017**, *425*, 765–775. [CrossRef]
192. Morawski, A.W.; Kusiak-Nejman, E.; Wanag, A.; Kapica-Kozar, J.; Wróbel, R.J.; Ohtani, B.; Aksienionek, M.; Lipińska, L. Photocatalytic degradation of acetic acid in the presence of visible light-active TiO₂-reduced graphene oxide photocatalysts. *Catal. Today* **2017**, *280*, 108–113. [CrossRef]
193. Fu, C.-C.; Juang, R.-S.; Huq, M.M.; Hsieh, C.-T. Enhanced adsorption and photodegradation of phenol in aqueous suspensions of titania/graphene oxide composite catalysts. *J. Taiwan Inst. Chem. Eng.* **2016**, *67*, 338–345. [CrossRef]
194. Liu, J.; Wang, L.; Tang, J.; Ma, J. Photocatalytic degradation of commercially sourced naphthenic acids by TiO₂-graphene composite nanomaterial. *Chemosphere* **2016**, *149*, 328–335. [CrossRef] [PubMed]
195. Nosrati, R.; Olad, A.; Shakoori, S. Preparation of an antibacterial, hydrophilic and photocatalytically active polyacrylic coating using TiO₂ nanoparticles sensitized by graphene oxide. *Mater. Sci. Eng. C* **2017**, *80*, 642–651. [CrossRef] [PubMed]
196. Zhou, Q.; Zhong, Y.H.; Chen, X.; Liu, J.H.; Huang, X.J.; Wu, Y.C. Adsorption and photocatalysis removal of fulvic acid by TiO₂-graphene composites. *J. Mater. Sci.* **2014**, *49*, 1066–1075. [CrossRef]
197. Li, Z.-J.; Huang, Z.-W.; Guo, W.-L.; Wang, L.; Zheng, L.-R.; Chai, Z.-F.; Shi, W.-Q. Enhanced Photocatalytic Removal of Uranium(VI) from Aqueous Solution by Magnetic TiO₂/Fe₃O₄ and Its Graphene Composite. *Environ. Sci. Technol.* **2017**, *51*, 5666–5674. [CrossRef] [PubMed]

